Aluna: Larissa Vieira Valadão Matrícula: 17/0084108
Orientadora: Prof. Dra. Maria Emília Schutesky Della Giustina
Universidade de Brasília
Instituto de Geociências

Mineralogia e relação textural e microestrutural do minério tipo IOCG da mina do Salobo, Província Mineral de Carajás: revisão da sequência paragenética

Dissertação de mestrado

2019

O presente trabalho foi realizado com apoio da Coordenação de Aperfeiçoamento de Pessoal de Nível Superior - Brasil (CAPES)

Resumo

A gênese do depósito Salobo é complexa, contudo, estudos petrográficos e de química mineral, juntamente com dados bibliográficos acerca do depósito, permitem estabelecer uma sequência paragenética e de eventos para o depósito. Desse modo, propõe-se que a mineralização de Salobo é caracterizada por um evento fonte principal de mineralização (2,73 Ga), inserido em um contexto de formação de depósito do tipo IOCG. Esse evento é definido por enriquecimento inicial em sódio, seguido por enriquecimento cálcico-férrico e por fim brechação e formação do minério cujo mineral principal é calcopirita. A reativação da Zona de Cisalhamento Cinzento, à qual o depósito Salobo é espacialmente relacionado (2,5 Ga), promoveu recristalização e metamorfismo, formando magnetita xistos no centro da mega-estrutura sigmoidal do Salobo, que gradam para granada-biotita xistos rumo às bordas, relacionados a uma potassificação e silicificação concomitante à deformação. Por fim, evento de remobilização do minério aconteceu a partir da interação entre fluidos de baixa temperatura, ricos em F e CO_2 e o minério fonte e gerou minério cuja principal associação mineral é constituída por bornita, calcocita e magnetita.

Abstract

The geological evolution of Salobo Cu-Au deposit is complex, however petrographic and mineral chemistry studies on rock samples of Salobo Mine, when coupled with the available scientific knowledge on the area, provide enough evidence to stablish an event and paragenetic sequence for the deposit. Salobo's mineralization is characterized by a 2.73 Ga mineralization event that originated the IOCG-type ore concentration. It is defined by an initial Na-enrichment, followed by Ca-Fe-enrichment and finally brecciation and precipitation from a S- and metal-rich fluid forming a chalcopyrite-rich ore. The reactivation of the Cinzento Shear Zone, when a transcurrent fault system that cuts the deposit was formed, resulted in the metamorphism of the Salobo rocks, forming a magnetite schist in the inner part of the sigmoidal mega-structure, which grades to a garnet-biotite schist towards its rims. Finally, extensive remobilization of the ore occurred by low-temperature F- and CO_2-rich fluids that interacted with the source ore concentration using the transcurrent fault system and resulted in the formation of ore constituted mainly by bornite, chalcocite and magnetite.

Dedicatória

A todas às geocientistas que, antes de mim, contribuíram para a construção do conhecimento geológico e proporcionaram a possibilidade de que mulheres como eu, hoje, tenham acesso a ele.

Agradecimentos

Agradeço a todos que colaboraram para que essa dissertação fosse concluída. Professores da universidade de Brasília, orientadora, meus pais, irmãs e avós. Agradeço especialmente à minha esposa por todo apoio e ajuda durante esse processo nem sempre tranquilo. Agradeço CAPES que forneceu bolsa que permitiu que eu pudesse me dedicar ao mestrado, e espero que a atual situação política brasileira não tire essa oportunidade de outras pessoas.

Índice

1 Introdução

O depósito de Salobo é um depósito de ouro e cobre de classe mundial localizado no sudeste do Cráton Amazônico, próximo ao limite norte da Província Carajás, no Domínio Carajás (Figura 1). Descoberto em 1975, a mina somente entrou em operação em novembro de 2012. Possui reserva estimada de 1.112 Mt, com 0,69 wt% Cu e 0,43 g/t Au (VALE, 2012). No terceiro trimestre de 2018, foram produzidas 50 mil toneladas de cobre contido em concentrado e no segundo trimestre de 2018, foram produzidas 46,7 mil toneladas (VALE, 2018).

Salobo é um depósito do tipo IOCG (*iron oxide copper-gold*; Huhn e Nascimento, 1997; Requia e Fontboté, 1999) inserido na Zona de Cisalhamento Cinzento (ZCC), que resulta na deformação milonítica intensa e morfologia verticalizada do depósito. Em função de reativações da ZCC, há dificuldade de identificação dos protólitos; assim, as classificações, tanto das rochas hospedeiras quanto do tipo de depósito têm sido reinterpretadas algumas vezes ao longo do tempo (Huhn e Nascimento, 1997; Lindenmayer, 2003, 1990; Melo et al., 2017). Originalmente, as rochas hospedeiras foram consideradas como formações ferríferas em um depósito do tipo vulcano-exalativo que teria sido metamorfizado em condições de alto grau (Lindenmayer, 1990). Contudo, Tassinari et al., (2003) consideram que a mineralização é hidrotermal, inicialmente gerada por volta de 2.7 Ga com remobilização em eventos posteriores. Já Melo et al., (2017) dizem que a mineralização principal do tipo IOCG ocorreu em 2,5 Ga, e está hospedada em rochas gnáissicas do Complexo Xingu (2,950 ± 25 e 2,857 ± 6,7 Ga) e granitoides da Suíte Igarapé Gelado (2,763 ± 4,4 Ga). Além disso, a alteração hidrotermal de Salobo incluiria, ainda segundo Melo et al. (2017), uma fase inicial de alteração sódico-cálcica (hastingsita e actinolita associada à allanita, escapolita e calcopirita) e silificação, seguidos por enriquecimento em ferro (grunerita, almandina, turmalina, faialita, magnetita, estilpnomelano, Fe-pirosmalita e greenalita), alteração potássica (biotita), mineralização, posterior hidratação dos silicatos de ferro (estilpnomelano, chamosita e greenalita) alteração pós-mineralização (hematita e feldspato potássico).

O minério é formado por diferentes litotipos com bornita, calcocita, magnetita, quantidades menores de calcopirita e ouro, além de conter quantidades significativas de Co, Ni, As, Ag, Mo e ETR (Melo, 2014). Ao contrário do depósito de Salobo, os demais depósitos IOCG da Província Carajás têm como mineral de minério predominante a calcopirita. Isso indica uma condição de estabilidade de sulfetos contrastante entre Salobo e os outros depósitos (Melo, 2014; Xavier et al., 2012). No minério de alto teor, o par bornita – calcocita, de maneira geral, apresenta textura mimerquítica/simplectítica caracterizando uma baixa temperatura de formação, <335ºC (Craig e Scott, 1974; Requia, 1995).

Características como: a associação incomum de minerais de minério, existência de múltiplos litotipos mineralizados e não relacionados entre si, evidências geocronológicas de múltiplos

eventos (Machado et al., 1991; Melo et al., 2017; Requia et al., 2003; Tassinari et al., 2003) de mineralização e feições indicativas de atuação de metamorfismo (Lindenmayer, 1990; Requia, 1995) tornam fundamental a reavaliação da sequência paragenética baseado em exposições recentes na Mina do Salobo. Assim, pretende-se discutir a relação entre deformação – metamorfismo – remobilização e upgrade do minério. Essas questões motivam a elaboração do presente trabalho, em que está colocada a hipótese de que a associação bornita – calcocita representa um evento posterior de remobilização metamórfica do minério original, constituído por magnetita-calcopirita. O foco do projeto, portanto, é a investigação mineralógico-textural do minério da mina do Salobo a fim de caracterizar as principais paragêneses e discutir a evolução geológica do depósito no Neoarqueano-Paleoproterozóico.

2 Contexto Geológico

A Província Carajás é situada na porção sudeste do Cráton Amazônico, o qual constitui uma das maiores áreas cratônicas do mundo. Ao norte da Província Carajás se localiza o Domínio Bacajá (2,670-2,07 Ga), a oeste está o Domínio Iriri-Xingu (1,90-1,86 Ga), ao sul o Domínio Santana do Araguaia e a leste a Faixa Araguaia (0,85-0,75 Ga; Melo et al., 2017; Santos, 2003; Vasquez et al., 2008). A Província é dividida em dois domínios tectônicos (Figura 1): o Domínio Carajás, ao norte, e o Domínio Rio Maria, ao sul. O Domínio Rio Maria é um terreno granito-greenstone com ocorrência de granitos, greenstone belts e rochas máficas e ultramáficas (Feio et al., 2013; Pollard et al., 2018; Vasquez et al., 2008). Já o Domínio Carajás (Figura 1) se caracteriza por embasamento mesoarqueano e sequências intrusivas e supracrustais neoarqueanas. As rochas do embasamento do Domínio Carajás são gnaisses tonalíticos, trondhjemiticos, granodioríticos e migmatitos do Complexo Xingu (idade de cristalização do protólito de 3066 ± 6,6 Ma; Silva, 2014), ortogranulitos máficos a félsicos do Complexo Pium (cristalização do protólito em 3002 ± 14 Ma; Pidgeon et al., 2000). Essas rochas foram afetadas por metamorfismo de alto grau em aproximadamente 2,85 Ga (Machado et al., 1991; Pidgeon et al., 2000; Pollard et al., 2018). Unidades composicionalmente distintas foram mais recentemente individualizadas por trabalhos de Moreto (2013, 2010), Moreto et al. (2011) e Feio et al. (2013) dentro do Complexo Xingu: (1) o Tonalito Bacaba (3,0 Ga), (2) Granito Canaã dos Carajás (2,96 Ga) e (3) os Granitos Serra Dourada e Cruzadão e Trondhjemito Rio Verde (2,87-2,86 Ga).

Depositadas sobre as rochas do embasamento há sequências metavulcanosedimentares portadoras de formações de ferríferas dos Grupo Rio Novo e Supergrupo Itacaiúnas, com idades entre 2,76 e 2,74 Ga (DOCEGEO, 1988; Hirata et al., 1982; Machado et al., 1991; Pinheiro, 1997; Pollard et al., 2018).

O Supergrupo Itacaiúnas compreende quatro grupos: (1) Grupo Igarapé Salobo, (2) Grupo Igarapé Pojuca, (3) Grupo Grão Pará e (4) Grupo Igarapé Bahia (DOCEGEO, 1988). Metabasaltos,

andesitos, metatraquiandesitos, quantidades menores de tufos e derrames metarriolíticos, formações ferríferas e unidades metassedimentares são as rochas que compõem tais grupos. Essas unidades foram depositadas na Bacia Carajás, formada em ambiente intra-cratônico (Gibbs et al., 1986; Olszewski et al., 1989). Essa bacia teria sido intensamente deformada sob transpressão regional a altas temperaturas em 2,85 Ga e sob transtensão rúptil regional por volta de 2,8 a 2,7 Ga, momento em que as rochas teriam se acomodado na estrutura sigmoidal de Carajás (Domingos, 2009; Holdsworth and Pinheiro, 2000; Pinheiro, 1997; Pinheiro and Holdsworth, 1997) As Zonas de Cisalhamento Cinzento e Carajás foram formadas durante esse processo, mas já foram propostos diversos momentos de reativação depois de 2,7 Ga (Domingos, 2009; Holdsworth and Pinheiro, 2000; Pinheiro and Holdsworth, 1997). A inversão tectônica da bacia teve início por volta de 2,7 Ga e durou até aproximadamente 2,6 Ga (Domingos, 2009).

Complexos máfico-ultramáficos, tais como Complexo Luanga (2763 ± 6 Ma), Suíte Cateté e Suite Serra Leste, intrudem as unidades metavulcanossedimentares e contêm mineralizações de níquel e EGP (Ferreira Filho et al., 2007; Machado et al., 1991).

Essas unidades estão parcialmente recobertas por coberturas siliciclásticas mais novas representadas por siltitos, arenitos com estratificação hummocky preservada, conglomerados, pelitos com estratificação plano-paralela, mármore dolomítico e filito carbonoso da Formação Águas Claras (Nogueira et al., 1995), que foi depositada em ambiente de plataforma marinha influenciada por tempestades a ambiente fluvial entrelaçado.

No Domínio Carajás os principais eventos de granitogênese são: (1) granitoides tipo A no Neoarqueano (~ 2.75–2.70 Ga - Granitos Estrela, Planalto, Plaquê, Serra de Rabo, Sossego, Curral, por exemplo; Barros et al., 2009; Feio et al., 2012; Huhn et al., 1999; Sardinha et al., 2006), (2) os Granitos *Old* Salobo e Itacaiúnas em ~2,57 Ga (Machado et al., 1991; Souza et al., 1996) e (3) no Paleoproterozoico em ~1,88 Ga granitos tipo A (Granitos Carajás, Young Salobo, Breves e Cigano, por exemplo; Machado et al., 1991; Souza et al., 1996).

O Granito Formiga, que é neoproterozóico (idade de cristalização 600-550 Ma; Grainger et al., 2008), também intrude o Domínio Carajás. O Granito Formiga possivelmente representa o magmatismo granítico mais jovem da região, mas a província também foi afetada por outros eventos magmáticos que correspondem a diques de diabásio, diorito e gabro tardios e não deformados (Xavier et al., 2012).

2.1 Depósitos IOCG na Província Carajás

Todos os depósitos tipo IOCG da Província Carajás estão no Domínio Carajás. É nele que se encontra a maior concentração conhecida de depósitos IOCG de classe mundial, com 100-789 Mt a 0,77-1,4% de Cu e 0,28-0,86 g/t de Au (Melo, 2014; Moreto et al., 2015a, 2015b; Xavier et al., 2012). As diferentes características dos depósitos IOCG de Carajás, como associações de alteração hidrotermal e minerais de minério distintos em cada um deles, são consequência de interações fluido-rocha e fluido-fluido, níveis crustais e rochas hospedeiras diversas (Melo, 2014). Os depósitos apresentam significativas alterações férrica e potássica, representadas por diferentes proporções de feldspato potássico, biotita, faialita, grunerita, actinolita, magnetita e clorita (Pollard et al., 2018). Os minerais de minério incluem combinações de calcopirita, bornita, calcocita, cobaltita, molibdenita e ouro que são normalmente associados à fluorita, apatita e

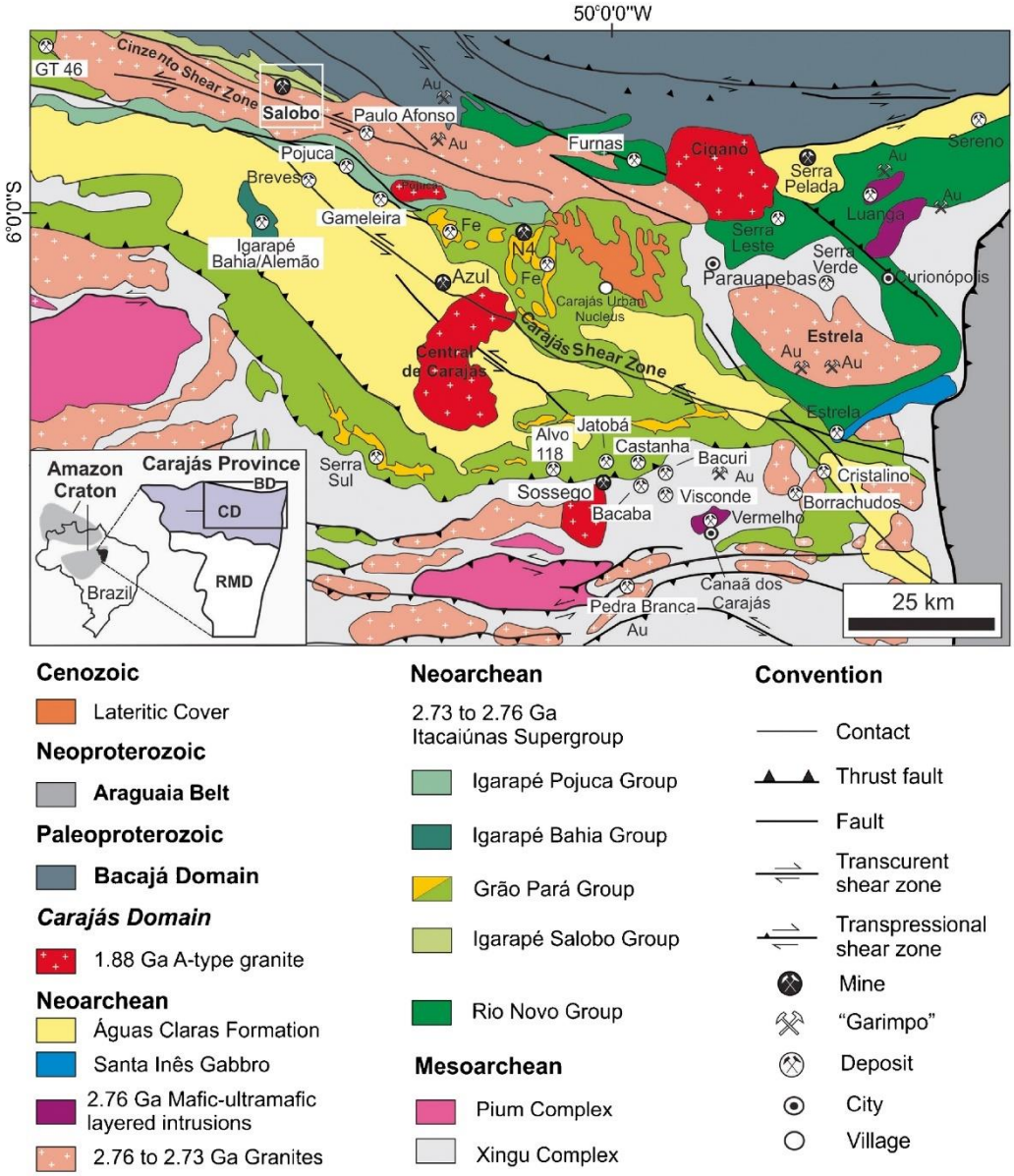

Figura 1 – Mapa Geológico do Domínio Carajás com destaque para os principais depósitos minerais retirado de Melo et al, (2017) apud Vasquez et al. (2008).

turmalina. Os depósitos apresentam assembleias sulfetadas de baixo enxofre e é comum serem pobres em quartzo, com enriquecimento em ETRL e enriquecimento variável de Co, Ni, Pb e Zn (Grainger et al., 2008; Pollard et al., 2018). Esses depósitos são localizados principalmente em dois setores, sul e norte, e têm relação espacial com grandes zonas de cisalhamento da região.

No setor sul depósitos como Sequeirinho, Cristalino, Visconde, Castanha, Bacaba, Jatobá e Bacuri se localizam ao longo da Zona de Cisalhamento Canaã. Essa é uma zona de cerca de 130 km de extensão, com *trend* E-W a WNW-ESE (Moreto et al., 2015b; Xavier et al., 2012). Esses depósitos definem o Cinturão Sul do Cobre (Moreto, 2013). Possuem também evolução paragenética da alteração hidrotermal parecida, em que a alteração sódica é seguida por alteração sódico-cálcica, potássica, formação de magnetita, cloritização/epidotização, mineralização e sericitização tardia. Essa sequência é identificada na maioria dos depósitos do Cinturão Sul (alguns corpos do depósito Sossego e nos alvos Castanha, Bacaba, Bacuri e Jatobá; Melo, 2014) o que pode indicar terem se formado em nível crustal profundo a intermediário. O minério é, normalmente, composto por calcopirita, pirita e magnetita e ocorre em corpos brechados e com halos das alterações hidrotermais (Melo, 2014). A natureza das rochas hospedeiras desses depósitos é diversa e inclui rochas intrusivas félsicas e máficas e, em menor quantidade, unidades metavulcanossedimentares do Supergrupo Itacaiúnas (Moreto et al., 2015b).

No setor norte os depósitos estão próximos ao limite com o Domínio Bacajá, relacionados à Zona de Cisalhamento Cinzento. O Lineamento Cinzento é uma zona transcorrente sinistral que se estende em um *trend*, em geral, de direção E-W (Pinheiro and Holdsworth, 1997; Xavier et al., 2012) e está espacialmente relacionada aos depósitos Salobo, Alvo GT-46 e Grota Funda (Hunger et al., 2018; Moreto et al., 2015b). Os depósitos do Setor Norte definem o Cinturão Norte do Cobre, onde os principais minerais de minério são calcopirita, bornita e/ou calcocita que comumente aparecem em lentes e corpos de sulfeto paralelos à foliação milonítica. Os corpos mineralizados mostram intensa alteração potássica de alta temperatura e condições dúcteis, enriquecimento em ferro, cloritização tardia e presença de turmalina (Lindenmayer, 2003; Moreto et al., 2015b; Requia et al., 2003).

2.2 Geocronologia dos depósitos tipo IOCG de Carajás

As idades encontradas na literatura para os depósitos do tipo IOCG de Carajás são com frequência de interpretação complexa, já que várias delas estão disponíveis para cada depósito (Xavier et al., 2012). Contudo, algumas são recorrentes em depósitos de ambos os setores.

No Cinturão Sul do Cobre (Tabela 1), idades U-Pb em monazita hidrotermal indicam que o sistema IOCG tenha sido formado entre 2,72 – 2,68 Ga nos depósitos Bacuri e Bacaba (Moreto et al., 2015b). Valores obtidos para os depósitos Visconde (2747±140 Ma) e Cristalino (2700±29 Ma) são semelhantes embora sejam pouco precisas (Pb-Pb em calcopirita; Moreto et al., 2015b;

Silva et al., 2012; Soares et al., 2001). Além disso, uma idade de mineralização posterior, em 2388±5 Ma, foi publicada por Pollard et al. (2018) para o depósito Cristalino. Os resultados por volta de 2.7 Ga são também próximos aos obtidos para a Suíte Planalto (2729 ± 17 Ma, 2710 ± 10 Ma e 2706± 5 Ma) por Feio et al. (2012) e para os depósitos Sequeirinho (2712 ± 5 Ma; U-Pb em monazita) e Pista (2685 ± 11 Ma e 2710 ± 11 Ma) por Moreto et al. (2015b).

Na porção norte do Domínio Carajás, o depósito GT-46 (Tabela 2) teve pelo menos dois estágios de mineralização distintos (de Freitas Toledo et al., 2019). O primeiro estágio é associado a uma mineralização disseminada controlada por estruturas dúcteis (2718 ± 56 Ma, Re-Os em molibdenita) enquanto o segundo estágio de veios e brechas foi datado em 2600 ± 8 Ma (Re-Os em molibdenita; (Silva et al., 2005). Alteração hidrotermal tardia com valor próximo a 2,5 Ga também são observadas no depósito (de Freitas Toledo et al., 2019). Também na porção norte, o minério de Grota Funda foi datado em 2530 ± 60 Ma (Re-Os em molibdenita; Hunger et al., 2018).

Já em Salobo (Tabela 2) Tassinari et al. (2003), em análises Pb-Pb em calcocita, turmalina, calcopirita e magnetita, obtiveram resultados que variam de aproximadamente 2,7 a 2,1 Ga. A idade de mineralização, segundo esses autores, seria de 2705±42 Ma, enquanto idades mais jovens de 2587±150 Ma e 2427±130 Ma, teriam relação com reativações da Zona de Cisalhamento Cinzento e a de 2112±12 Ma em cristais tardios de magnetita seria relacionada a um evento hidrotermal associado a metamorfismo de baixo grau. Contudo, autores como Melo et al. (2017) e Requia et al. (2003) interpretam resultados de cerca de 2,5 Ga para a mineralização (2579±71 Ma, Pb-Pb em bornita e calcopirita e 2535±8,4 Ma, U-Pb em zircão; respectivamente) como sendo sincrônicas à intrusão do Granito *Old* Salobo (2573±2 Ma, U-Pb em zircão; Machado et al., 1991). Por fim, Melo (2018) sugere também que idades relativas à Zona de Cisalhamento Cinzento (2555±4 Ma; Machado et al., 1991) e mineralização (2452 ± 14, U-Pb em monazita; Melo, 2014), significam que, pelo menos em Salobo, a gênese do depósito tem relação com as sucessivas reativações da zona de cisalhamento sobre o qual ele se localiza, possivelmente com pulsos hidrotermais associados.

Tabela 1 – Tabela com dados geocronológicos do Cinturão Sul do Domínio Carajás.

Depósitos IOCG do Cinturão Sul do Cobre				
Depósito	**Rocha/Mineral**	**Idade (Ma)**	**Método**	**Referência**
Sossego				
Corpo Sossego				
	Rochas hospedeiras			
	Granito granofírico de Sossego	2740 ± 26	U-Pb, em zircão	Moreto et al. (2015b)
	Minério			
	Calcopirita de brecha mineralizada	1592 ± 45	Pb-Pb, em calcopirita	Neves (2006)
	Brecha mineralizada	1879 ± 4.1	U-Pb,em monazita	Moreto et al. (2015b)
	Brecha mineralizada	1904 ± 5.2	U-Pb,em monazita	Moreto et al. (2015b)
Sequeirinho Orebody				
	Rochas hospedeiras			
	Granito Sequeirinho	3014 ± 22	U-Pb, em zircão	Moreto et al. (2015b)
	Granito Sequeirinho	3010 ± 21	U-Pb, em zircão	Moreto et al. (2015b)
	Granito Sequeirinho	2989 ± 5.2	U-Pb, em zircão	Moreto et al. (2015b)
	Gabronorito	2739 ± 5.9	U-Pb, em zircão	Moreto et al. (2015b)
	Minério			
	Anfibólio relacionado ao minério	2199 ± 13	$^{40}Ar/^{39}Ar$, em anfibólio	Marschik et al. (2003)
	Calcopirita de minério maciço	2530 ± 25	Pb-Pb, em calcopirita	Neves (2006)
	Calcopirita de minério maciço	2608 ± 25	Pb-Pb, em calcopirita	Neves (2006)
	Brecha mineralizada	2578 ± 29	Sm-Nd, rocha total	Neves (2006)
	Brecha mineralizada	3076 ± 5.3	U-Pb, em zircão	Moreto et al. (2015b)
	Brecha mineralizada	2712 ± 4.7	U-Pb,em monazita	Moreto et al. (2015b)
Pista Orebody				
	Rochas hospedeiras			
	Rocha félsica metavulcânica	2968 ± 15	U-Pb, em zircão	Moreto et al. (2015b)
	Rocha félsica metavulcânica	2979 ± 5.3	U-Pb, em zircão	Moreto et al. (2015b)
	Minério			
	Rocha metavulcânica silicificada	2685 ± 11	Re-Os, em molibdenita	Moreto et al. (2015b)
	Rocha metavulcânica com alteração sódica	2710 ± 11	Re-Os, em molibdenita	Moreto et al. (2015b)
Curral Orebody				
	Rochas hospedeiras			
	Granito Curral	2739 ± 4.2	U-Pb, em zircão	Moreto et al. (2015b)
	Minério			
	Brecha mineralizada	1890 ± 8.5	U-Pb,em monazita	Moreto et al. (2015b)
Cristalino				
	Rochas hospedeiras			
	Diorito Cristalino	2738 ± 6	U-Pb, em zircão	Huhn et al. (1999b)
	Granito Planalto	2747 ± 2	U-Pb, em zircão	Huhn et al. (1999b)
	Granito Planalto	2710 ± 10	U-Pb, em zircão	Feio et al. (2012)
	Granito Planalto	2706 ± 5	U-Pb, em zircão	Feio et al. (2012)
	Granito Planalto	2733 ± 2	U-Pb, em zircão	Feio et al. (2012)
	Granito Planalto	2731 ± 1	U-Pb, em zircão	Feio et al. (2012)
	Granito Planalto	2738 ± 3	U-Pb, em zircão (SHRIMP)	Feio et al. (2013)
	Granito Planalto	2730 ± 5	U-Pb, em zircão (SHRIMP)	Feio et al. (2013)
	Minério			
	Veio com biotita-quartzo-calcopirita-pirita	2388 ± 5	$^{40}Ar/^{39}Ar$, em biotita	Pollard et al. (2018)
	Brecha mineralizada	2700 ± 29* (*MSWD=656)	Pb-Pb, em calcopirita e pirita	Soares et al. (2001)
Bacaba				
	Tonalito Bacaba	3001 ± 3.6	U-Pb, em zircão	Moreto et al. (2011)
	Granito Serra Dourada[1]	2860 ± 22	U-Pb, em zircão	Moreto et al. (2011)
	Granito Serra Dourada	2848 ± 5.5	U-Pb, em zircão	Moreto et al. (2015a)
	Minério			
	Granito Serra Dourada com alteração sódica	2720 ± 15	U-Pb, em zircão	Moreto et al. (2015a)
	Monazita de brecha mineralizada	2060 ± 9.6	U-Pb, em zircão	Moreto et al. (2015a)
		2681 ± 20	U-Pb, em zircão	Moreto et al. (2015a)
Bacuri				
	Minério			
	Alteração clorítica (relatcionada à mineralização)	2703 ± 6.2	U-Pb,em monazita	Moreto et al. (2015a)
	Veio de molibdenita cortando Granito Serra Dourada	2758 ± 11	Re-Os, em molibdenita	Moreto et al. (2015a)
Visconde				
	Rochas hospedeiras			
	Pórfiro quartzo-feldspático	2741 ± 4.7	U-Pb, em zircão	Moreto et al. (2015a)
	Minério			
	Brecha mineralizada	2747 ± 140	Pb-Pb, em calcopirita	Silva et al. (2012)

1Granito Serra Dourada também hospeda os depósitos Bacuri e Visconde.

Tabela 2 – Tabela com dados geocronológicos reunidos para os depósitos do Cinturão Norte do Cobre de Carajás.

Depósitos IOCG do Cinturão Norte do Cobre				
Depósito	**Rocha/Mineral**	**Idade (Ma)**	**Método**	**Referência**
GT-46				
	Rochas hospedeiras			
	Granito não deformado	2557 ± 26	U-Pb, em zircão	de Freitas Toledo et al. (2019)
	Tonalito foliado	2532 ± 26	U-Pb, em zircão	de Freitas Toledo et al. (2019)
	Pegmatito	2588 ± 38	U-Pb, em zircão	de Freitas Toledo et al. (2019)
	Granito cinza	2612 ± 2	U-Pb,em monazita	Silva et al. (2005)
	Granodiorit foliado	2639 ± 16	U-Pb, em zircão	de Freitas Toledo et al. (2019)
	Granitos rosa e cinza e granitos com granada	2652 ± 98	Sm-Nd, rocha total	Silva et al. (2005)
	Granitos rosa e cinza	2668 ± 100	Sm-Nd, rocha total	Silva et al. (2005)
	Basaltos e gabro	2686 ± 87	Sm-Nd, rocha total	Silva et al. (2005)
	Anfibolito (cristalização do protólito igneo)	2774 ± 19	U-Pb, em zircão	de Freitas Toledo et al. (2019)
	Minério			
	Biotita (alteração potássica)	1858 ± 7	$^{40}Ar/^{39}Ar$, em biotita	Silva et al. (2005)
	Molibdenita de pegmatito	2449 ± 44	Re-Os, em molibdenita	de Freitas Toledo et al. (2019)
	Molibdenita de rocha intensamente cloritizada	2503 ± 51	Re-Os, em molibdenita	de Freitas Toledo et al. (2019)
	Molibdenita de rocha pegmatítica	2554 ± 8	Re-Os, em molibdenita	Silva et al. (2005)
	Molibdenita de rocha pegmatítica	2557 ± 8	Re-Os, em molibdenita	Silva et al. (2005)
	Molibdenita de granito	2600 ± 8	Re-Os, em molibdenita	Silva et al. (2005)
	Molibdenito de anfibolito	2711 ± 9	Re-Os, em molibdenita	Silva et al. (2005)
	Molibdenita de anfibolito	2718 ± 56	Re-Os, em molibdenita	de Freitas Toledo et al. (2019)
Grota Funda				
	Minério			
	Molibdenita de veios de grunerita e magnetita	2530 ± 60	Re-Os, em molibdenita	Hunger et al. (2018)
Salobo				
	Rochas hospedeiras			
	Rocha rica em magnetita	2551 ± 2	U-Pb,em monazita	Machado et al. (1991)
	Rocha rica em anfibólio	2497 ± 5	U-Pb, in titanite	Machado et al. (1991)
	Granito Old Salobo	2547 ± 5.3	U-Pb, em zircão	Melo et al. (2017)
	Rocha rica em anfibólio	2555 ± 4/–3	U-Pb, em zircão	Machado et al. (1991)
	Granito Old Salobo	2573 ± 2	U-Pb, em zircão	Machado et al. (1991)
	Rocha rica em anfibólio	2581 ± 5	U-Pb, in titanite	Machado et al. (1991)
	Gnaisse Cascata	2701 ± 30	U-Pb, em zircão	Melo et al. (2017)
	Veio granítico (metamorfismo)	2732	U-Pb, em titanita	Machado et al. (1991)
	Veio granítico	2758	U-Pb, em zircão	Machado et al. (1991)
	Anfibolito foliado (metamorfismo)	2761 ± 3	U-Pb, em zircão	Machado et al. (1991)
	Gnaisse Cascata	2763 ± 4.4	U-Pb, em zircão	Melo et al. (2017)
	Rochas com alteração pós-mineralização	2950 ± 25	U-Pb, em zircão	Melo et al. (2017)
	Minério			
	Lixiviado de magnetita	2112 ± 12	Pb-Pb, em magnetita	Tassinari et al. (2003)
	Lixiviado de calcopirita	2427 ± 130	Pb-Pb, em calcopirita	Tassinari et al. (2003)
	Minério de Salobo	2452 ± 14	U-Pb,em monazita	Melo et al. (2017)
	Minério de Salobo	2535 ± 8.4	U-Pb, em zircão	Melo et al. (2017)
	Molibdenita	2562 ± 8	Re-Os, em molibdenita	Requia et al. (2003)
	Molibdenita	2576 ± 8	Re-Os, em molibdenita	Requia et al. (2003)
	Lixiviados de bornita e calcocita	2579 ± 71	Pb-Pb, em bornita calcocita	Requia et al. (2003)
	Lixiviados de turmalina	2587 ± 150	Pb-Pb, em turmalina	Tassinari et al. (2003)
	Lixiviados de calcocita	2705 ± 42	Pb-Pb, in calcocita	Tassinari et al. (2003)

2.3 Depósito de Salobo: estado da arte

O depósito de Salobo situa-se na a Zona de Cisalhamento Transcorrente do Cinzento, de direção WNW-ESE e se localiza próximo ao limite norte do Domínio Carajás, da Província Carajás (Figura 1; Vasquez et al., 2008). O depósito é intensamente deformado, verticalizado e afetado por alteração hidrotermal (Melo, 2014). Por conta dessas características houve dificuldade para identificar os protólitos e as classificações, tanto das rochas hospedeiras quanto do tipo de depósito, foram reinterpretadas algumas vezes ao longo do tempo (DOCEGEO, 1988; Huhn and Nascimento, 1997; Lindenmayer, 2003, 1990; Melo et al., 2017; Requia and Fontboté, 2000).

Lindenmayer (1990), concluiu que a sequência hospedeira de Salobo (Sequência Salobo) é formada por basaltos metamorfisados, formações ferríferas, grauvacas, arenitos arcosianos a arcósios que estão colocados sobre um embasamento de trondhjemitos e menos frequentemente de gnaisses graníticos. Esses anfibolitos, ou seja, basaltos metamorfisados, apresentam composição com enriquecimento em Fe, LILE e LREE, típicos de rochas basálticas continentais, similares às do Grupo Grão Pará. Foi considerada também a presença de dois tipos de formação ferrífera que formariam ciclos sedimentares com as metagrauvacas. Essas rochas seriam parte do Grupo Grão Pará e teriam sido formadas em 2759±2 Ma. Dois corpos graníticos intrudem a sequência, o Granito *Old* Salobo (granito sódico, alcalino e metaluminoso deformado e intrudido sob condições mesozonais) e o Granito *Young* Salobo (álcali-feldspato quartzo sienito, potássico e metaluminoso não deformado e intrudido sob condições epizonais). A sequência Salobo, ainda segundo Lindenmayer (1990), foi submetida a metamorfismo progressivo de caráter termal a condições próximas a fácies piroxênio *hornfels* (~750ºC), seguido por dois episódios de alteração hidrotermal (que teriam ocorrido por volta de 2,5 Ga relacionados com a reativação da Zona de Cisalhamento Cinzento ao fim) coerentes com fácies anfibolito (~650ºC) e xisto verde (370ºC). O metamorfismo progressivo se distingue por assembleia mineral praticamente anidra nos litotipos, tais como faialita, hastingsita, almandina e magnetita, plagioclásio cálcico e quartzo. O primeiro evento hidrotermal seria marcado pela destruição da faialita e da hastingsita e pela albitização do plagioclásio, resultando em assembleias de grunerita, almandina, magnetita, biotita, quartzo, cummingtonita, albita, biotita e silimanita. O segundo evento hidrotermal se distingue por intensa cloritização de minerais ferro-magnesianos. Os sulfetos de cobre predominantes no minério são bornita-calcocita com calcopirita em menor quantidade, além de terem sido identificados molibdenita, ouro, saflorita e cobaltita (Lindenmayer, 1990). Lindenmayer e Fyfe (1994) propõem uma reinterpretação da gênese do depósito sugerindo uma formação mista em que a magnetita teria uma origem singenética e o enriquecimento em ouro, molibdênio, urânio, flúor e REE teria acontecido por influência de fluidos magmáticos-hidrotermais em 1,8 Ga (colocação das suítes tipo A). Basearam-se para a proposta na alteração hidrotermal associada a enriquecimento de FeOt, K, Ce, Th, U e REE, e na presença de uraninita, fluorita, molibdenita, calcopirita e ouro em veios tardios mineralizados. Finalmente os protólitos do depósito foram reinterpretados (Lindenmayer, 2003) como predominantemente metavulcânicos derivados de rochas dacíticas e basálticas.

Posteriormente, Requia (1995), ao abordar a influência do metamorfismo e fases fluidas na gênese da mineralização de Salobo, interpretou que as rochas teriam passado por metamorfismo de fácies anfibolito alto (650ºC, temperatura menor que a proposta por Lindenmayer, 1990) seguido por apenas um evento hidrotermal análogo a metamorfismo de fácies xisto verde alto (347ºC). Nesse contexto, durante a alteração metamórfica, a assembleia sulfetada provavelmente teria sido um

solução sólida cúbica, rica em cobre, em equilíbrio com a solução sólida da bornita, que em condições metamórficas de fácies xisto verde evoluiu para calcopirita tetragonal (estável abaixo de 547ºC) e bornita-calcocita, provenientes da solução sólida da bornita (<335ºC; Requia, 1995). A combinação de ouro rico em cobre, cobaltita, sulfetos de cobre e veio de clorita, com o intervalo de estabilidade do ouro e cobaltita (<400ºC), indica associação entre o evento magmático hidrotermal de baixa temperatura e os fluidos responsáveis pela presença de cobre e ouro. Fluidos estudados no depósito apresentam indicativo de mistura, sendo o responsável pela mineralização um fluido aquoso de salinidade elevada que se associou ao evento metamórfico-hidrotermal de baixa temperatura, com possíveis fontes sendo águas de formação, águas meteóricas que se tornaram salinas por reações de hidratação retrógradas ou fontes magmáticas (Requia, 1995).

A partir da observação de um processo de albitização precoce seguido de alteração potássica, e da associação da mineralização em Salobo com intrusões plutônicas félsicas de 2,5 Ga, o depósito foi incluído na classe dos depósitos tipo IOCG (Huhn and Nascimento, 1997). Já Lindenmayer e Teixeira, 1999 ao discutir o modelo genético proposto para Salobo, comparam o depósito tanto a modelos IOCG quanto a depósitos pórfiro Cu-Au,. Requia e Fontboté (1999) observaram que a maior parte dos óxidos de ferro que compõe as antes chamadas formações ferríferas eram na verdade de origem epigenética e associadas a sistema hidrotermal. As rochas teriam sido afetadas por um intenso metassomatismo alcalino que tinham primeiramente uma composição com modificações químicas pouco expressivas e valores enriquecidos de cálcio (anfibólio cálcico e plagioclásio cálcico), depois uma alteração sódica (expressa pela substituição de plagioclásio cálcico por sódico), seguido por intenso metassomatismo potássico (expresso pela substituição parcial ou total do plagioclásio por feldspato potássico e pela formação de biotita (Requia e Fontboté, 2000). Enxofre de origem magmática e a distribuição da alteração hidrotermal em direção a uma área central também foram evidências consideradas para a determinação de Salobo como sendo um depósito IOCG (Requia and Fontboté, 2000).

Datação Re-Os em molibdenita associada aos sulfetos (2576±8 Ma) dá um valor coerente com a do Granito *Old* Salobo, o que levou a se sugerir que a formação do depósito se deu por causa da colocação do mesmo (Requia et al., 2003). Outro modelo, proposto por Tassinari et al. (2003) a partir de idades Pb-Pb em calcocita (2705+42 Ma), turmalina (2587+150 Ma), calcopirita (2427+130 Ma) e magnetita (2112+12 Ma), indica que a evolução metalogenética do depósito se deu em pelo menos três estágios: (1) deposição singenética de cobre primário durante o vulcanismo e deposição do Grupo Igarapé Salobo em 2,7 Ga, (2) reequilíbrio e mobilização causada pelo desenvolvimento do sistema *strike-slip* Carajás-Cinzento e colocação do Granito *Old* Salobo e (3) um estágio tardio de retrometamorfismo de fácies xisto verde em 2,1 Ga.

Uma nova sequência de alteração hidrotermal, espacialmente relacionada ao desenvolvimento da Zona de Cisalhamento Cinzento, é proposta por Melo (2014) , segundo a que o sistema teria

evoluído de um estágio de alteração sódico-cálcica (representado por hastingsita-actinolita), seguida por estágio de enriquecimento em ferro (grunerita-almandina-faialita) e formação de turmalina. Na sequência houve alteração potássica com biotita, que foi acompanhada pela formação de magnetita cogenética ao minério (Melo, 2014). Alteração hidrotermal pós-mineralização (feldspato potássico, alteração propilítica e formação de hematita) afeta as zonas mineralizadas e é relacionada à colocação do Granito *Old* Salobo (Melo, 2014). As rochas hospedeiras foram reclassificadas como sendo predominantemente quartzo-feldspáticas (anfibolitos e formações ferríferas ou rochas ricas em óxidos de ferro assumem caráter hidrotermal) e os protólitos seriam então gnaisses do Complexo Xingu (2,950±25 Ma) e da Suíte Igarapé Gelado (2,763±4,4 Ma; (Melo, 2014)). Os principais eventos que teriam influenciado a formação do depósito Salobo seriam: (1) cristalização e deformação dos granitoides da Suíte Igarapé Gelado junto com ativação da Zona de Cisalhamento Cinzento, metamorfismo dinâmico, circulação de fluidos, metassomatismo e mineralização, (2) reativação no Arqueano tardio da Zona de Cisalhamento com remobilização de minério e formação da pós-mineralização associada ao Granito *Old* Salobo e (3) magmatismo anorogênico (*Young* Salobo) e evento termal tardio (Melo, 2014). Desse modo, a mineralização IOCG não estaria relacionada à intrusão do granito *Old* Salobo, uma vez que seus padrões de alteração hidrotermal são distintos (Melo, 2014).

A proposta anterior de sequência paragenética é revisada em Melo et al. (2017): a alteração sódico-cálcica de alta temperatura é seguida por silicificação, enriquecimento em ferro, formação de turmalina, alteração potássica com biotita, formação do minério de cobre e ouro, alteração por silicatos hidratados ricos em ferro e, por fim, todos esses estágios teriam sido sobrepostos por alteração pós-mineralização de feldspato potássico contendo hematita e propilítica (Melo et al., 2017). Além de rochas do Complexo Xingu e Suíte Igarapé Gelado, também são identificadas rochas remanescentes do Grupo Igarapé Salobo (Melo et al., 2017). Coletivamente, os dados acerca do Depósito de Salobo refletem uma história evolutiva complexa, com eventos hidrotermais se superpondo, mas o estágio principal de mineralização teria ocorrido junto com a intrusão de *Old* Salobo e reativação da Zona de Cisalhamento Cinzento (Melo et al., 2017).

3 Artigo

A review of the hydrothermal alteration stages in the giant metamorphosed IOCG Salobo deposit, Carajás Mineral Province, Brazil

Introduction

Terranes affected by metamorphism and tectonism are host to many of the world's largest metallic ore deposits, where deformation, metamorphism and associated fluids can both form and modify them. Metamorphic remobilization causes modification involving mass transfer processes during deformation and reconcentration of an ore deposit of economic interest (Marshall et al., 1998; Marshall and Gilligan, 1993). Deformation, in response to deviatoric stress, is an intrinsic part of the remobilization during regional metamorphism and plays a critical role in mixed- and liquid-state transfer processes (Marshall et al., 1998). Most extensive remobilization happens through either liquid-state or mixed-state mass transfer and the liquid phase is typically of hydrothermal origin, and may include deeply circulating meteoric, dewatering, metamorphic and magmatic fluids (Marshall et al., 1998). The consequences of aqueous flow remobilization are systems of dilatational veins and/or replacements and related rock alterations that may be syn- or post-tectonic (Marshall et al., 1998).

The Salobo deposit is a Cu-Au IOCG (iron oxide copper-gold) deposit (Huhn and Nascimento, 1997) located near the Cinzento Shear Zone (CSZ) in the northern limit of the Carajás Mineral Province (Amazon Craton, Brazil). The deposit is structurally controlled, show well-developed mylonitic foliation and its morphology is nearly vertical (Lindenmayer, 1990). The ore of Salobo is formed mainly by bornite, chalcocite and magnetite, with minor chalcopyrite, and with high contents of Co, Ni, As, Ag, Mo and REE (Melo et al., 2017). The Salobo is the only IOCG deposit at Carajás that has such association of bornite-chalcocite as the high-grade ore. The Salobo mine began operating in November 2012 and has an estimated reserve of 1.112 Mt, with 0,69 wt% of Cu and 0,43 g/t of Au (VALE, 2012). During the third trimester of 2018, the mine produced 50 thousand tons of concentrated copper and during the second trimester of 2018 it produced 46,7 thousand tons of concentrated copper were produced (VALE, 2018).

Because of its location, at a shear zone that has been reactivated multiple times, the rocks are usually highly deformed and have hydrothermal alteration, which made it difficult to identify the deposit protoliths. Therefore, the host rocks classifications and the deposit type were reinterpreted a few times throughout time (Huhn and Nascimento, 1997; Lindenmayer, 2003, 1990; Melo et al., 2017). Originally, the host rocks were thought to be iron formations of a VMS deposit that suffered high grade metamorphism (Lindenmayer, 1990). However, Tassinari et al., (2003) considered the ore to have an hydrothermal origin and to be generated around 2.7 Ga, with later remobilization events. On the other hand, (Melo et al., 2017) states that the main IOCG mineralization event occurred around 2.5 Ga and is hosted in gneissic rocks of the Xingu Complex (2.950 ± 25 and 2.857 ± 7 Ga) and granitoids of the Igarapé Gelado Suite (2.763 ± 4 Ga).

In a recent review of the paragenetic sequence (Melo et al., 2017), a few inconsistencies showed up, especially regarding the relation between the gangue and the ore assemblage. The metamorphic-deformational history was disregarded and, accordingly, the hydrothermal alteration in Salobo would have multiple alteration stages, but consisting of only one mineralization event. In such, bornite solid-solution is transformed into a fine symplectitic intergrowth of digenite-chalcocite, which indicates that it was formed at relatively low temperatures in the Cu-Fe-S system (<335°C; Craig and Scott, 1974; Requia, 1995). However, this lower temperature association has been considered paragenetic to high temperature minerals and in the same mineralization event. This inconsistency, together with evidences for multiple events that affected the mineralization, as recorded by different ages found in many studies (Machado et al., 1991; Melo et al., 2017; Requia et al., 2003; Tassinari et al., 2003) make it essential to reassess the paragenetic sequence of the Salobo deposit, considering the effects of thermal imprint, remobilization, deformation and metamorphism.

Based on the above, this study presents a different view of the paragenetic sequence and further recrystallization events that might have been involved in the remobilization of the Salobo ore through time. This study was conducted from samples collected at recent exposures at the Salobo Mine, including petrography, SEM imaging and EPMA major and minor mineral chemistry analysis. The combined mineralogical-textural investigation of Cu-Fe sulfides represents the first description of chalcopyrite breccia in the Salobo deposit, similar to other deposits in the Carajás Province. This approach, based on the equilibrium conditions of ore minerals, made it possible to discuss the events superimposed to the Salobo deposit, which resulted from a multi-stage evolution that includes at least three episodes of recrystallization/remobilization. Finally, we discuss dating problematics and suggest a review of the evolution of the deposit, from the Neoarchean towards the Rhyacian-Orosirian.

Geological Context

IOCG deposits at Carajás Province

Basement rocks of the Carajás Domain (CD) are tonalitic, trondhjemitic and granodioritic gneisses and migmatites of Xingu Complex (protolith crystallization age of 3066 ± 6.6 Ma; Silva, 2014) and mafic and felsic orthogranulites of Pium Complex (protolith crystallization age of 3002 ± 14 Ma; Pidgeon et al., 2000). High grade metamorphism affected these complexes around 2.85 Ga (Machado et al., 1991; Pidgeon et al., 2000; Pollard et al., 2018). Over the basement rocks, metavolcano-sedimentary sequences, hosting giant banded iron formations, of Rio Novo Group and Itacaiúnas Supergroup were deposited between 2.76 to 2.74 Ga (DOCEGEO, 1988; Machado et al., 1991; Pollard et al., 2018). Those units are partially covered Águas Claras Formation (Nogueira et al., 1995).

The main regional events of widespread granitic magmatism are: (1) at the Mesoarchean, around 3.0 Ga (p.e. Bacaba Tonalite; Moreto et al., 2011), (2) Neoarchean age type-A granitoids of 2.75-2.70 Ga (p.e. Estrela, Planalto, Plaquê, Serra do Rabo, Sossego and Curral granites; Barros et al., 2009; Feio et al., 2012; Huhn et al., 1999; Sardinha et al., 2006), (3) ~2.57 Ga Old Salobo and Itacaiúnas Granites (Machado et al., 1991; Souza et al., 1996) and (4) Paleoproterozoic, 1.88 Ga, type-A granites (p.e. Carajás, Young Salobo, Breves and Cigano granites; (Machado et al., 1991; Souza et al., 1996).

All IOCG deposits of the Carajás Province are located at CD, and they represent the biggest known concentration of world-class IOCG deposits, containing more than 8 billion tonnes of ore at 0.77-1.4% Cu and 0,28-0.86 g/t Au (Moreto et al., 2015b, 2015a, 2015a; Xavier et al., 2012; Xavier et al., 2017).

IOCG deposits are hosted on basement rocks and Itacaiúnas Supergroup. These deposits are located at two different sectors of the CD, northern and southern, and they present a spatial relationship with regional-scale shear zones.

The southern sector hosts deposits like Sequeirinho, Cristalino, Visconde, Castanha, Bacaba, Jatobá e Bacuri are located around Canaã Shear Zone. Canaã is a shear zone of about 130km of extension and an E-W to WNW-ESE trend (Moreto et al., 2015b; Xavier et al., 2012).

At southern sector, defined as the Southern Copper Belt (Moreto, 2013), the deposits present a similar paragenetic evolution of the hydrothermal alteration, where the sodic alteration is followed by sodic-calcic alteration, potassic alteration, magnetite formation, chlorite and epidote alterations, mineralization and later sericitic alteration. This sequence is identified in most deposits at the Southern Copper Belt: some ore bodies at Sequeirinho, as well as Cristalino, Castanha, Bacaba, Bacuri, Visconde and Jatobá deposits (Melo, 2014). The ore at the southern belt deposits is generally composed of chalcopyrite, pyrite and magnetite and occurs in brecciated bodies that have alteration halos associated to them. The nature of the host rocks is diverse and includes intrusive felsic and mafic rocks and, in minor quantities, meta-volcano sedimentary rocks of Itacaiúnas Supergroup (Moreto et al., 2015b).

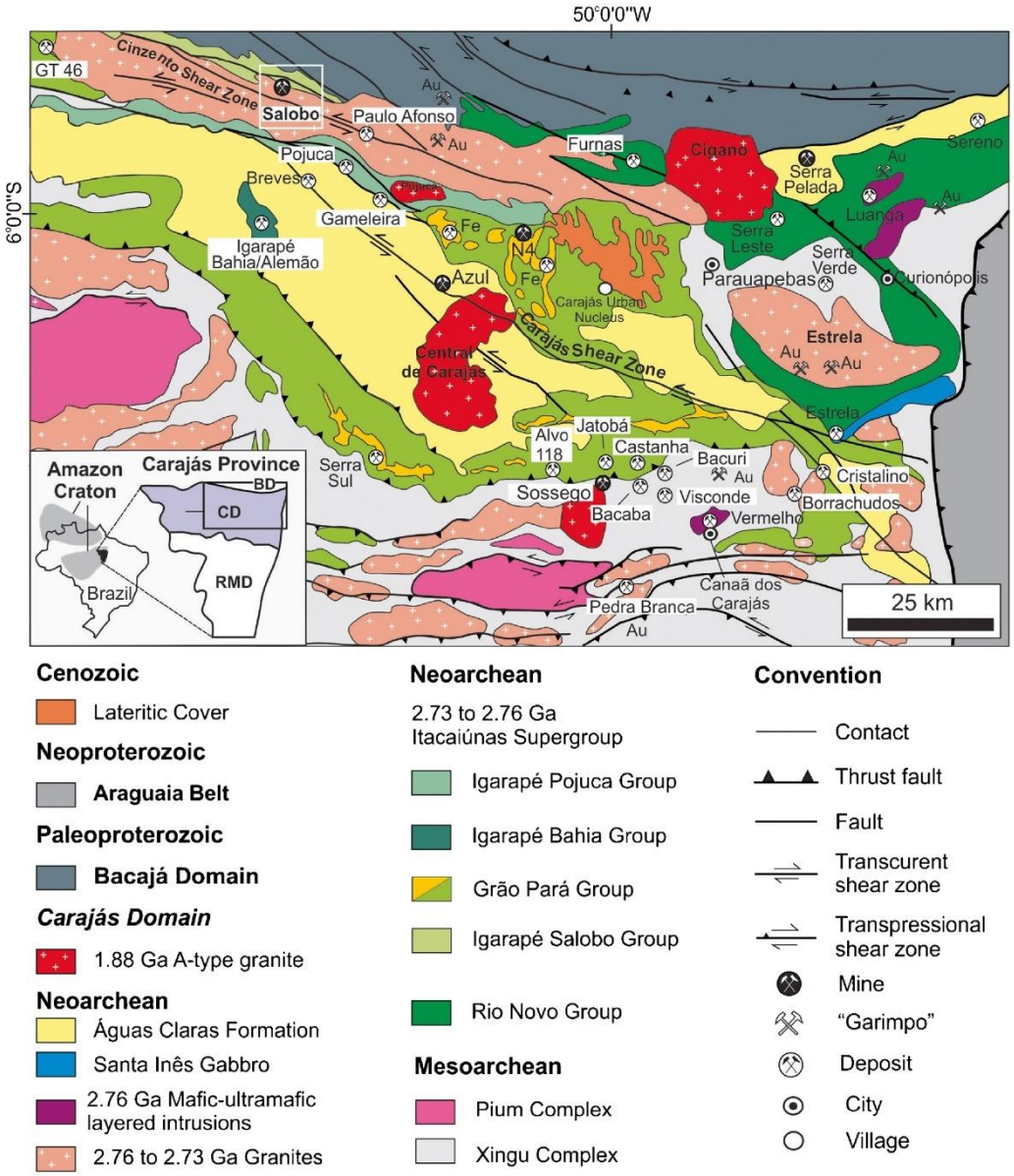

Figure 1 - Carajás Mineral Province geologic map modified from Melo et al. (2017) apud Vasquez et al. (2008).

At the northern sector the deposits are located near the Bacajá Domain limit and are related to the Cinzento Shear Zone. The Cinzento lineament is a transcurrent sinistral zone that has an E-W trend (Pinheiro and Holdsworth, 1997; Xavier et al., 2012) and is spatially associated with the Salobo, GT-46 and Grota Funda deposits (Moreto et al., 2015b). At the Northern Copper Belt, the main ore minerals are chalcopyrite, bornite and/or chalcocite that usually form lenses and sulfide ore bodies parallel to the mylonitic foliation. The ore bodies are highly affected by high temperature potassic alteration and show tourmaline (Lindenmayer, 2003; Moreto et al., 2015b; Requia et al., 2003).

The Salobo deposit – Previous works

The Salobo Deposit is located at the Cinzento Shear Zone, a transcurrent fault of WNW-ESE direction, near the northern limit of the Carajás Domain, at Carajás Province. The deposit is intensely deformed, with vertical morphology and pervasive hydrothermal alteration (Melo, 2014). Intense metamorphism and hydrothermal influence overprint most of the deposit and, initially, made it difficult to identify and accurately classify the deposits host rocks and its protoliths, and even the deposit type has been reinterpreted a few times (Huhn and Nascimento, 1997; Lindenmayer, 2003, 1990; Melo et al., 2017; Requia and Fontboté, 2000).

Lindenmayer (1990) concluded that the host sequence (The Igarapé Salobo Group) is formed by metamorphosed basalts, banded iron formations, greywackes, arkosic arenites to arkoses that are deposited over a trondhjemitic basement and less frequently gneissic granites. The amphibolites are enriched in Fe, LIL and LREE, typical of continental basaltic rocks and comparable to the Grão Pará Group. The rocks considered as iron formations were further divided in two types that formed sedimentary cycles along with the metagraywackes, forming part of the Grão Pará Group.

Two granitic bodies are considered intrusive into the sequence, the Old Salobo Granite (sodic, alkaline and metaluminous deformed granite that intruded in mesozonal conditions) and the Young Salobo Granite (potassic and metaluminous alkali-feldspar quartz syenite that is not deformed and intruded at epizonal conditions). The Igarapé Salobo Group, still according to Lindenmayer (1990), would have been affected by thermal progressive metamorphism up to conditions close of that of pyroxene hornfels facies (~750 °C), followed by two events of hydrothermal alteration that occurred around 2.5 Ga, culminating in an Cinzento Shear Zone reactivation at the end of these events. The progressive metamorphism was distinguished by the anhydrous assembly, such as fayalite, hastingsite, almandine and magnetite, calcic plagioclase and quartz. The hydrothermal events were considered to be coherent with amphibolite (~650 °C) and, then, greenschist (370 °C) facies. The first hydrothermal event was marked by the fayalite and hastingsite disappearance and by the albitization of plagioclase, resulting in grunerite, almandine, magnetite, biotite, quartz, cummingtonite, albite and sillimanite assembly. The second hydrothermal event is distinguished by intense chloritization processes of Fe-Mn minerals. The

hydrothermal provenience of Cu was indicated by a positive correlation between Fe and Cu. The predominant ore minerals are bornite and chalcocite with minor chalcopyrite as well as some molybdenite, gold, safflorite and cobaltite (Lindenmayer, 1990).

Lindenmayer and Fyfe (1994) propose a first reinterpretation of the ore deposit genesis and suggest a syngenetic origin for magnetite and a magmatic-hydrothermal origin for fluids that caused Au, Mo, U, F, and REE enrichment at ~1.8 Ga, time of widespread type A granite intrusions at Carajás Province. This proposal was based on the association between hydrothermal alteration to FeOt, K, Ce, Th, U, and REE-enrichment and the presence of uraninite, fluorite, molybdenite, chalcopyrite and gold in late-forming ore veins. Finally, the deposit protoliths were also reinterpreted (Lindenmayer, 2003) as predominantly metavolcanics rocks derived from dacitic and basaltic rocks.

Afterwards, Requia, (1995) when assessing the metamorphism and the role of fluid phases in the ore genesis at the Salobo deposit stated that the rocks would have attained amphibolite facies metamorphism (650 °C), a lower temperature than the one proposed by Lindenmayer, 1990) followed by only one green-schist facies hydrothermal event (~350 °C). In this context, during metamorphism, the sulfide assembly probably formed a copper-rich cubic solid solution in equilibrium with the bornite solid solution and evolved to tetragonal chalcopyrite (stable under 547 °C) and bornite-chalcocite, provenient from the bornite solid solution under 335 °C (Requia, 1995). The combination of copper-rich gold, cobaltite, copper sulfides and chlorite veins, with the stability of gold and cobaltite (<400 °C) indicated an association between the magmatic-hydrothermal event of low-temperature and the fluids responsible for Cu and Au in the system. Requia (1995) also studied fluid inclusions that indicate mixing of fluids and account the mineralization to a high-salinity aqueous fluid that was associated to the greenschist metamorphic-hydrothermal event. Possibly, this fluid originated from connate water, meteoric water that acquired high-salinity due to retrograde hydration reactions or even from magmatic fluids (Requia, 1995).

From the observation of an early albitization process followed by potassic alteration and from the association of the Salobo mineralization to plutonic felsic intrusions of 2.5 Ga, the deposit was included at the IOCG deposits class (Huhn and Nascimento, 1997) as defined by Hitzman et al., (1992). Requia and Fontboté (1999) observed that the majority of the iron oxides that composed the so-called iron formations were in fact of epigenetic origin and were associated to a hydrothermal system. The rocks would have been affected by an intense alkaline metasomatism that initially had chemical composition with little modification and high calcium values (calcic amphiboles and calcic plagioclase), then a sodic alteration (materialized by the substitution of calcic plagioclase by sodic plagioclase), followed by intense potassic metasomatism (partial or total substitution of plagioclase by potassic feldspar and biotite formation; Requia and Fontboté,

2000). Magmatic sulfur and the distribution of the hydrothermal alteration towards a central area were also evidence that were considered in order to determine Salobo as being a deposit of the IOCG class (Requia and Fontboté, 2000).

Re-Os dating in molybdenite in paragenesis with copper sulfides (2576±8 Ma) yielded a value that is coherent with the Old Salobo Granite age, and so, it was proposed that the deposit formation was a result of the granite intrusion (Requia et al., 2003). Another model, proposed by Tassinari et al. (2003) based on a Pb-Pb ages in chalcocite (2705±42 Ma), tourmaline (2587±150 Ma), chalcopyrite (2427±130 Ma) and magnetite (2112±12 Ma), suggests three stages for the deposit evolution: (1) Syngenetic deposition of copper during the volcanism and sediment deposition of the Salobo Group at 2.7 Ga, (2) reequilibration and remobilization caused by the evolution of the strike-slip Carajás-Cinzento system and the intrusion of the Old Salobo Granite at 2.5 Ga, and (3) a late-stage retrograde metamorphism of greenschist facies at 2.1 Ga.

A new sequence of hydrothermal alteration, especially related to the Cinzento Shear Zone, was proposed by Melo (2014). In this sequence the system evolved from a sodic-calcic alteration (hastingsite-actinolite) to an iron enrichment and tourmaline formation stage (grunerite-almandine-fayalite and tourmaline). Then, the potassic alteration formed biotite along with cogenetic formation of magnetite and the ore (Melo, 2014). Post-ore hydrothermal alteration (potassic feldspar, propylitic alteration and hematite formation) affects the ore-rich zones and originated from the intrusion of Old Salobo Granite (Melo, 2014). The host rocks were reclassified as being predominantly made of quartz and feldspar while metavolcanics/amphibolites and iron-formations/iron oxide-rich rocks are characterized as being hydrothermally formed (Melo, 2014). Protoliths were also revised and considered to be part of the Xingu Complex (2.950±25 Ma) and the Igarapé Gelado Suite (2.763±4.4 Ma; Melo, 2014).

According to Metlo (2014), the main events to affect the genesis of Salobo deposit would, therefore, be: (1) crystallization and deformation of granitoids from the Igarapé Gelado Suite synchronically to Cinzento Shear Zone activation, dynamic metamorphism, fluid circulation, metasomatism and mineralization, (2) late-Archean reactivation of Cinzento Shear zone associated to ore remobilization and post-ore alteration associated with Old Salobo Granite intrusion, and (3) anorogenic magmatism (locally materialized by Young Salobo Granite but spread through the province) and late thermal event (Melo, 2014). So, the IOCG mineralization wouldn't be related to the granite intrusion, since they have distinct hydrothermal patterns (Melo, 2014).

However, in a more recent proposal of an alteration sequence and mineral paragenesis for Salobo deposit (Melo et al., 2017), the authors suggested a first sodic-calcic alteration, followed by silicification, iron-enrichment, tourmaline formation, potassic alteration (biotite, Cu-Au ore

formation), and, lastly, Fe-silicate hydration. Finally, all those stages were overprinted by post-ore alteration containing potassic feldspar, hematite and propylitic alteration (Melo et al., 2017). As well as Xingu Complex and Igarapé Gelado Suite, remnants from Igarapé Salobo Group were also identified as host rocks (Melo et al., 2017). The authors concludes that data on the Salobo Deposit reflect a complex evolution process where hydrothermal event are superimposed, but the main mineralization event probably occurred at the same time as the Old Salobo Granite intruded and the Cinzento Shear Zone was reactivated around 2.5 Ga (Melo et al., 2017).

Materials and methods

Characterization of the paragenetic sequence of hydrothermal alteration and mineralization in the Salobo deposit was carried out based on petrographic studies under transmitted and reflected light on forty four polished thin sections of sixteen samples collected from recent exposures at the Salobo Mine open-pit (Table 1). Scanning electronic microscope images (JEOL, JSM 7001F) in back-scattered mode were produced at Microscopy and Microanalysis Laboratory of the University of Brasília, Brazil. Mineral analyses were obtained by electron microprobe (JEOL, JXA8230) applying wavelength dispersive technique at the Microprobe Laboratory of the University of Brasília, Brazil. Operating conditions were an accelerating voltage of 15kV and probe current of 10nA for all elements except for As, Zn, Ga, Se, S, Pb, Bi, Cd, Te, Fe, Co, Cu, Ni, Mo, Au, Ag and Sb which were analyzed with accelerating voltages of 20kV and probe current of 20nA.

Table 1 – Samples table, showing lithotypes and which analytical methods were performed at each thin section of samples,

Sample	Lithotype	Thin Section	Analytical Methods		
			Petrography	EMP	SEM
1	Cpy Breccia	A	x	Sulfides	x
		B1	x	Silicates	
		B2	x		
2	Cpy Breccia	A	x	Sulfides	
		B	x	Silicates; Sulfides	x
3	Magnetite Schist	A	x	Sulfides	
		B	x	Sulfides	
		C	x		x
4	Cpy Breccia	A	x		
		B	x	Sulfides	
		C	x	Silicates; Sulfides	x
5	Cpy Breccia	A	x	Silicates; Sulfides	
		B1	x	Silicates	x
		B2	x		
6	Magnetite Schist	A	x	Sulfides	
		B	x		
		C	x	Sulfides	
		D	x	Sulfides	
7	Cpy Breccia	A	x	Silicates; Sulfides	x
		B	x	Sulfides	
		C	x	Sulfides	
		D	x	Sulfides	
101	Hydrothermaly altered granitic rock	A	x	Sulfides	
		B	x		
102	Hydrothermaly altered granitic rock	A	x		
		B	x	Sulfides	
103	Cpy Breccia	A	x	Silicates; Sulfides	
		B	x		
104	Cpy Breccia	A	x		
		B	x		
105	Cpy Breccia	A	x		
		B	x		
106	Hydrothermal Carbonate	A	x		
		B	x	Sulfides	
		C	x		
107	Magnetite Schist	A	x		
		B	x	Sulfides	
S1	Garnet-biotite schist	A	x		
		B	x		
		C	x		
S2	Garnet-biotite schist	A	x		
		B	x		

Results

Sample description

Samples from the Salobo mine include granitic rock with hydrothermal alteration (Figure a, b), hydrothermal breccia with magnetite breccia (Figure 2c), hydrothermal breccia with chalcopyrite matrix (Figure a), garnet-biotite schists (low grade ore; Figure b) and magnetite-rich schist (high grade ore; Figure c). The lithotypes differ on protoliths, type and intensity of hydrothermal processes and deformation conditions that generated them.

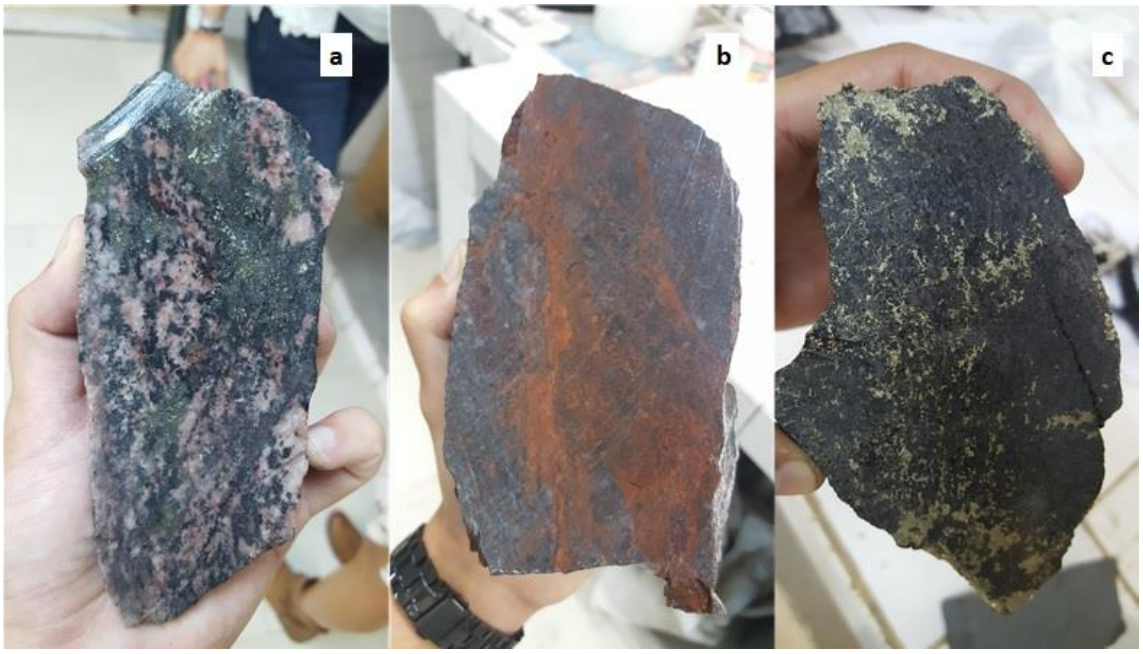

Figure 2 - Macroscopic ore samples from: a) granitic rock with hydrothermal alteration and chalcopyrite concentrations; b) granitic rock with hydrothermal alteration and red alteration; c) clast supported hydrothermal breccia with magnetite matrix;

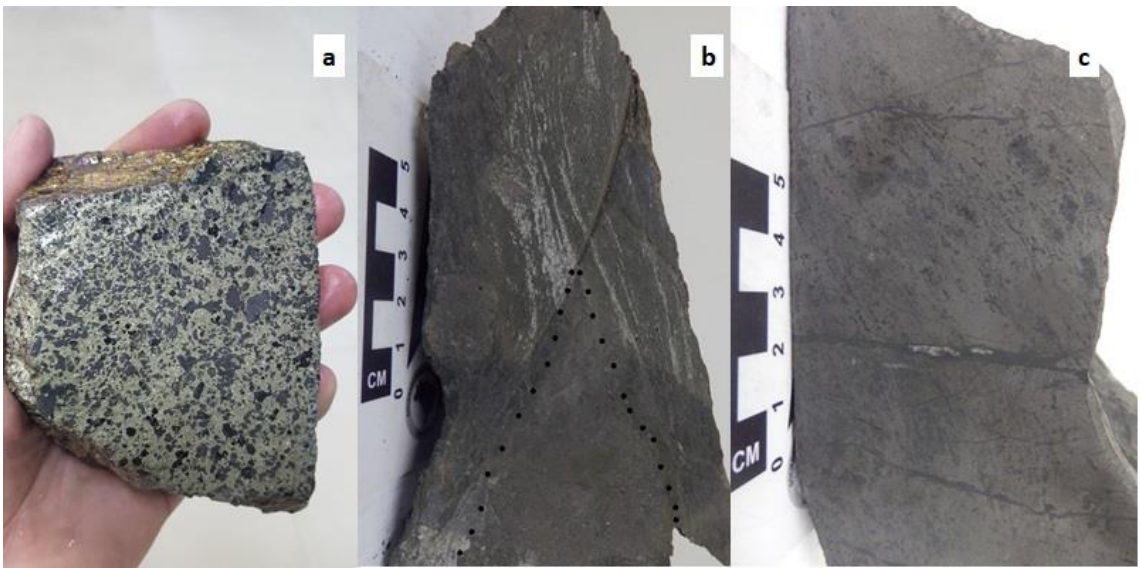

Figure 3 - Macroscopic samples of: a)) clast supported hydrothermal breccia with chalcopyrite matrix; b) garnet-biotite schist with highlighted (black points) garnet pressure shadow c) magnetite-rich schist where carbonate, bornite and fluorite veins are visible.

Granitic rocks with hydrothermal alteration and garnet-biotite schists contain only minor amounts of ore. Higher grade ore samples include magnetite-rich schist and hydrothermal amphibole breccia with chalcopyrite matrix.

At the Salobo mine the deformation is a result of Cinzento Shear Zone influence. The shear zone affects the deposit's host rocks to form vertical corridors of transcurrent faults. The ore is mostly structurally controlled and bound inside these corridors (Figure). This means that hydrothermally altered granitic rocks that host the mineralization are cut by vertical corridors of magnetic schists at the inner part and garnet biotite schists towards their rims, the high-grade and low-grade ore, respectively. Along these corridors, lens of amphibole-bearing breccia with chalcopyrite matrix and, eventually, granitic rocks, were preserved from much of reactivation stress of the Cinzento Shear Zone and presents a gradual, lateral transition to magnetitic schists.

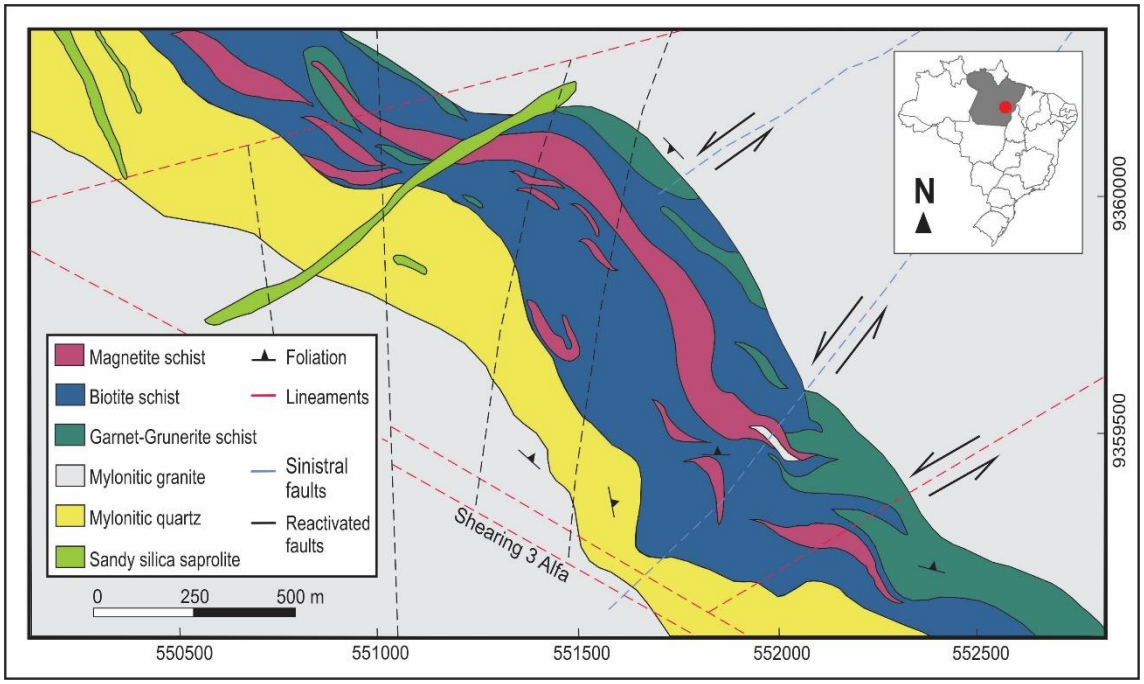

Figure 4 - Map of the Salobo Mine showing the main lithotypes of the mine.

Hydrothermally altered Granitic rock

Altered granitic rocks are fine- to- medium grained, depending in the degree of hydrothermal imprint. Color also varies, transitioning from red to a pinkish tonality and is lighter where less altered. Intercalation of mafic and felsic bands that define an incipient tectonic foliation is cut by either chalcopyrite-rich veins or bright red alteration on different portions of the samples (figure 2a, b).

The primary minerals are quartz, plagioclase and potassic feldspar, with minor quantities of biotite and accessory titanite. The texture is predominantly granoblastic with incipient formation of bands. Quartz grains have undulose extinction, bulges along boundaries, domains with sub-grain formation and recrystallization. Plagioclase also show undulose extinction and is saussuritized.

Potassic feldspar has some preserved pericline-albite twinning, undulose extinction and evidences of recrystallization.

The alteration of granitic rocks results in an assemblage of scapolite, tourmaline, quartz, k-feldspar, chlorite, calcite, epidote, apatite, allanita, poorly preserved amphiboles, magnetite, ilmenite, sericite and hematite, usually forming near to or filling veins. The first minerals appearing as alteration phases are scapolite and tourmaline. Then amphiboles, allanite, magnetite and apatite, which are later altered by other minerals such as chlorite, epidote and hematite. Bornite and chalcopyrite appear in interstices between grains and commonly have hematite boxwork overgrowths (**Erro! Fonte de referência não encontrada.**a, b). Late forming quartz veins are also present. However, it was possible to determine abundant fine-grained quartz, hematite, chlorite and other phyllosilicates forming the matrix around larger grains of quartz,

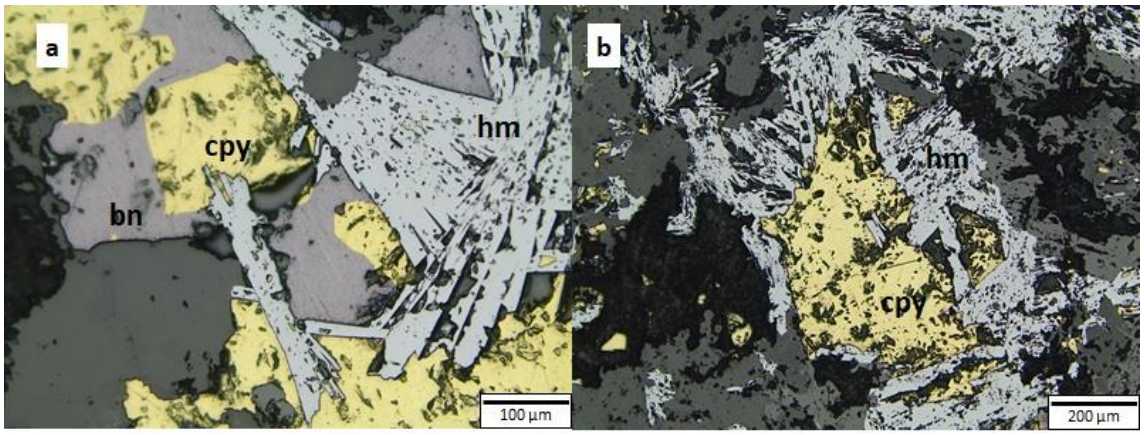

Figure 5 - Polished thin sections of hydrothermally altered granitic rock. a) Detail of boxwork hematite overgrowth on interstitial bornite and chalcopyrite. b) Boxwork hematite overgrowth on interstitial chalcopyrite. hem = Hematite; cpy = chalcopyrite; bn = bornite.

feldspar and chloritized biotite.

Magnetite breccia and Chalcopyrite breccia

Magnetite breccia and chalcopyrite breccia differ mainly in two aspects: the most abundant mineral that constitute their matrix and intensity of tectonic deformation. Magnetite breccia has a matrix composed mostly of magnetite while chalcopyrite breccia's matrix has predominant chalcopyrite. The change in the amount of chalcopyrite matrix and magnetite matrix is usually gradual, but in times, it can be abrupt and produce sharp contacts. An increase in magnetite matrix content is associated to an increase in deformation and at least two foliation planes are present where it is prevalent (Figure 6a to 6d).

Magnetite breccia is usually clast supported but presents matrix supported domains. It has variable amounts of matrix and minor chalcopyrite in its interstices, veins and fractures (Figure 7a and 7b). Magnetite breccia has a dark gray color that results from the combination of magnetite matrix and amphibole clasts (Figure 2c). Clasts tend to be rounder than the observed in chalcopyrite

matrix and vary in size from coarse to fine grained. Foliation and granoblastic textures are more common in portion richer in magnetite matrix.

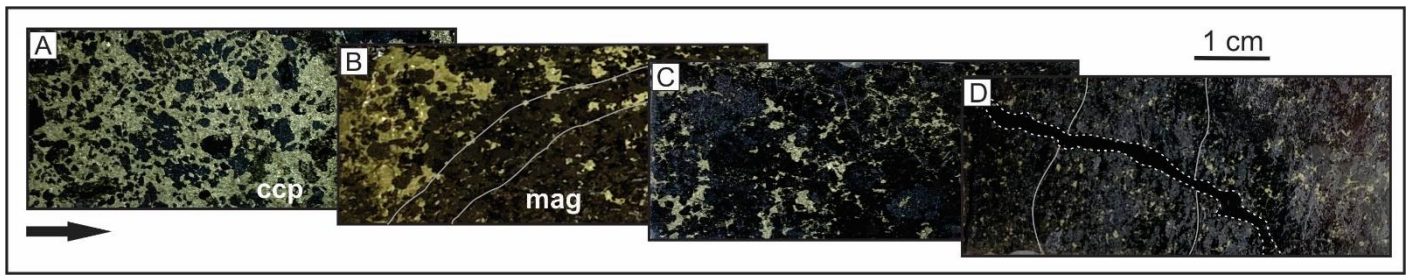

Figure 6 – Gradual change from high contents of chalcopyrite matrix and little tectonic deformation at chalcopyrite breccia to highly deformed magnetite breccia with little interstitial chalcopyrite and high contents of magnetite.

The chalcopyrite breccia (cpy-breccia) may contain variable amounts of matrix, being either matrix or clast supported. When the matrix is abundant, the rock assumes a yellow color because of chalcopyrite (Figure 3a). Matrix is mainly composed of chalcopyrite but has minor siegenite, pyrite, pyrrhotite, magnetite and traces of galena, sphalerite, bornite, uraninite and pentlandite. Clasts sizes and shapes are also variable, going from fine grained to pegmatoid and presenting round to sharp angled shapes.

The chalcopyrite breccia and magnetite breccia have the most diverse mineralogy of all the lithotypes sampled. Their mineralogy is similar and, besides magnetite and chalcopyrite, matrix

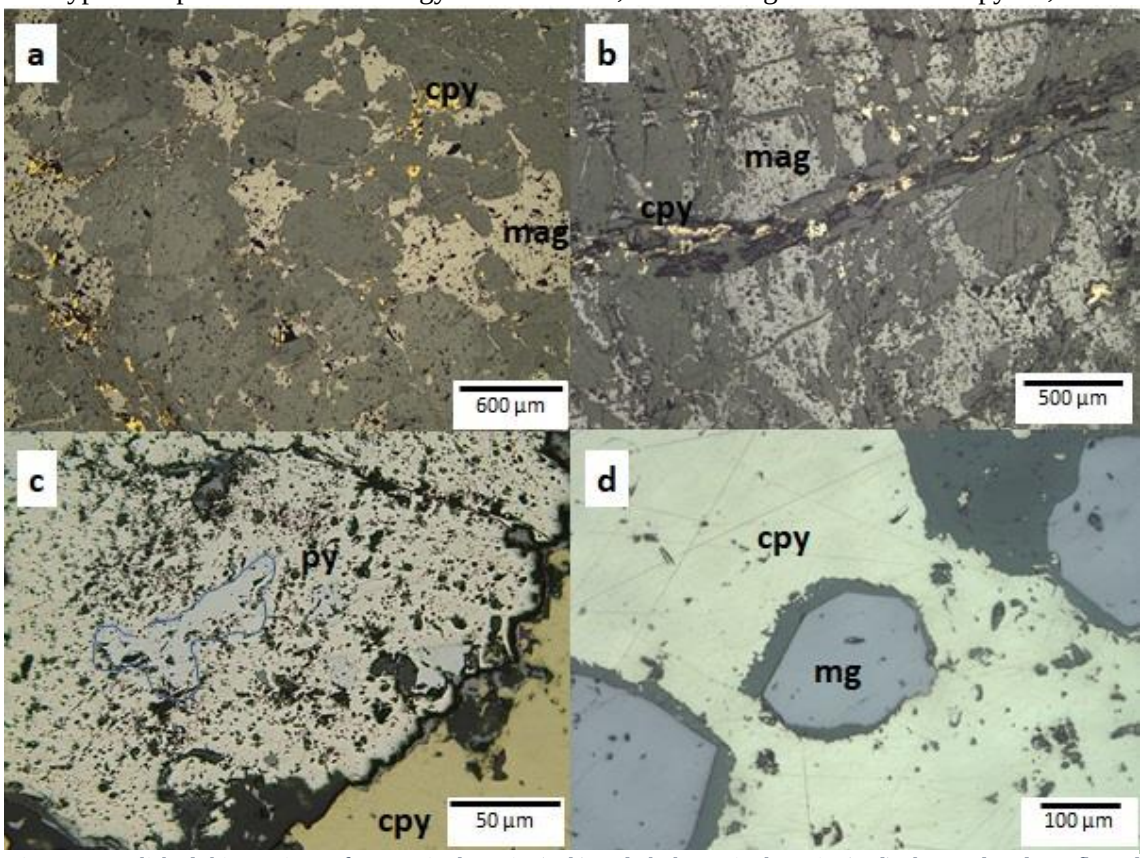

Figure 7 - Polished thin sections of magnetite breccia (a, b) and chalcopyrite breccia (c, d) observed under reflected light. a) Zone with predominant magnetite matrix around gangue clasts and little interstitial chalcopyrite. b) Very fractured magnetite breccia with a brittle vein containing chalcopyrite. c) Gray domains in pyrite crystal. The gray domain in the center is outlined (blue line). d) Phyllosilicate coating around magnetite clasts. Cpy = chalcopyrite, mg = magnetite, po = pyrrhotite, Ni-py = Nickel-rich pyrite, py = pyrite, sie = siegenite.

also includes minor siegenite, pyrite, pyrrhotite, as well as traces of galena, sphalerite, bornite, uraninite and pentlandite. There are magnetite, chalcopyrite, bornite and uraninite inclusions in several of the clasts. Clasts, in both cases, are made of actinolite (Figure 8b), grunerite, hornblende, apatite, ilvaite, epidote and allanita all of which are often altered to phyllosilicates (chlorite, stilpnomelane, Fe-pyrosmalite, greenalite) and oxides (hematite, magnetite, rutile). However, fayalite and traces of ferrossilite were identified only at zones with abundant magnetite matrix of the magnetite breccia. Grunerite is also preferentially formed on magnetite breccia. Grains of fayalite were in some cases very altered to chlorite and the characteristic high relief and interference colors facilitated identification.

At least three different amphiboles were observed and electronic microprobe analysis were necessary to distinguish between them. They are actinolite and hornblende (hastingsite and ferro-ferri-hornblende). Size and degree of preservation of amphiboles are variable and they can be millimetric to centimetric and either be very well preserved or completely altered by later hydrothermal events and weathering. However, hornblende appears altering both of the former amphiboles and is, generally, better preserved. Chlorite, pyrosmalite, stilpnomelane, sericite and (Figure 8b) other phyllosilicate minerals fill veins associated with fluorite and quartz (Figure 9a) and also partially substitute the higher temperature minerals such as amphiboles, and in magnetite breccia's case, fayalite and ferrossilite.

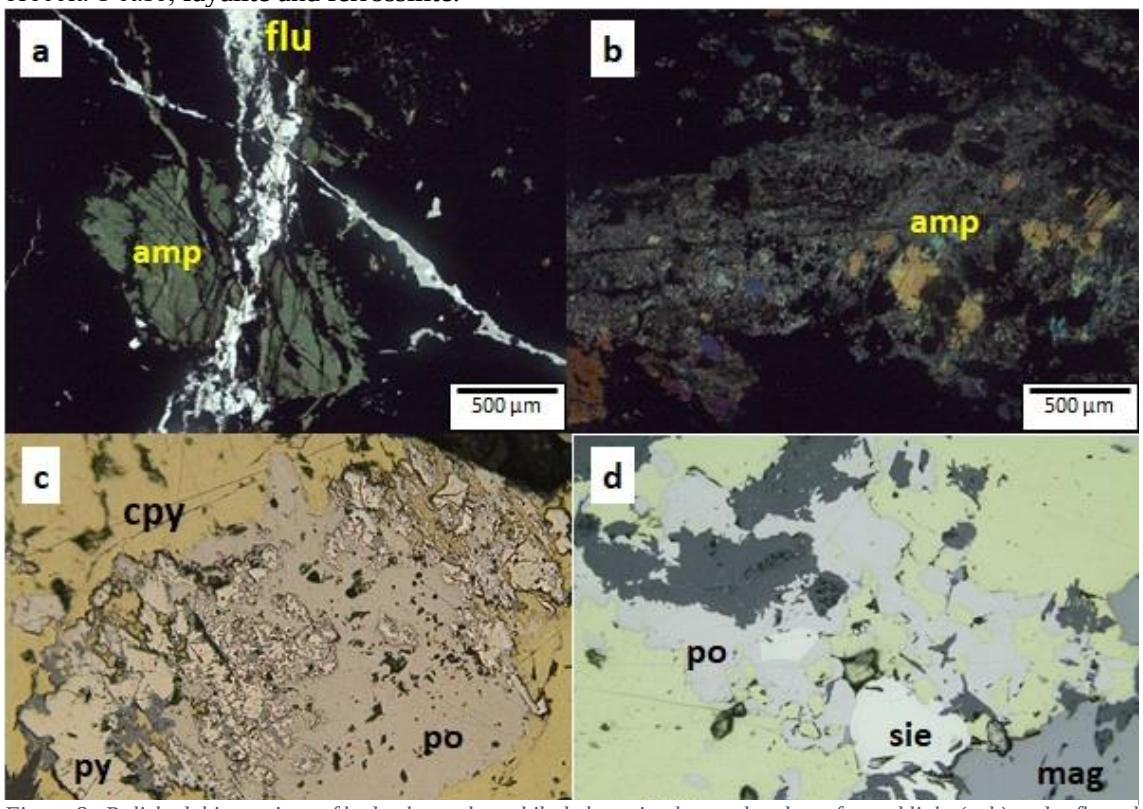

Figure 8 - Polished thin sections of hydrothermal amphibole breccia observed under refracted light (a, b) and reflected light (c and d). a) Hastingsite crystal cut by fluorite and quartz veins (P//); b) Very chloritized actinolite crystals (PX); c) Pyrite transforming into pyrrhotite, magnetite and hematite; d) Siegenite (light yellow) crystal associated to pyrrhotite (pinkish) that is placed along the contacts of silicates with the chalcopyrite matrix. amp = amphibole, cpy = chalcopyrite, mag = magnetite, po = pyrrhotite, py = pyrite.

Lamellar pentlandite exsolutions are rarely visible at the chalcopyrite matrix. Pyrite crystals are fractured, have absorption rims, straight edges and shows decomposition reactions to form pyrrhotite, magnetite and/or hematite (Figure 8c). Some zones of a slightly grayer color can be seen in pyrite grains (Figure 9c). Siegenite has round to anedral habits, high reflectivity, light yellow color and is associated to chalcopyrite and pyrrhotite presence (Figure 8d). Pyrrhotite has anedral habits and is usually located along the contacts of chalcopyrite matrix and silicate clasts or it may also appear as pyrite decomposition reaction result (Figure 8d).

Magnetite may either appear as (1) breccia matrix, (2) fractured and/or altered to hematite grains imbedded in chalcopyrite matrix, (3) filling rock fractures, (4) forming late, euhedral crystals, (5) as an alteration product placed along silicate cleavage planes and fractures or (6) as a result of pyrite decomposition. This diversity indicates multiple times of formation for magnetite. When forming clasts (2), magnetite grains commonly have a phyllosilicate border at its edges (Figure 8d). Another mineral with multiple formation times is hematite, that can either be a magnetite weathering product, fill cleavage planes and fractures at amphibole grains, contour limits of grains in contact with the matrix, as a product of a late stage hydrothermal alteration.

An indicative of deformation is apatite with undulose extinction and movement can be inferred from fluid textures where the crystals are extremely small, probably due to the strength of the fluid passage at the brecciation event.

Garnet-biotite schist

Garnet-biotite schist is dark colored due to biotite with dark gray with light shades corresponding to quartz- or garnet- rich domains. The schist bands are millimetric to centimetric intercalations of quartz and biotite that involve coarse grained round garnet with sigmoidal pressure shadows (Figure 3b).

The garnet-biotite schist is composed of quartz, biotite, garnet and magnetite with minor ilmenite, apatite, plagioclase, chlorite, bornite, fluorite and hematite. Schistosity planes are marked by aligned biotite crystals alternated with recrystallized quartz domains (Figure 9a). Biotite is sometimes chloritized. Garnet crystals are coarse grained and show a syntectonic inner foliation, with biotite, magnetite and quartz inclusions. Pressure shadows are present around these grains. A euhedral and inclusion-free outer rim in garnet overgrowing the foliation evidences a post-kinematic second-stage growth. Fractures in garnet contain quartz, feldspar, biotite, ilmenite and

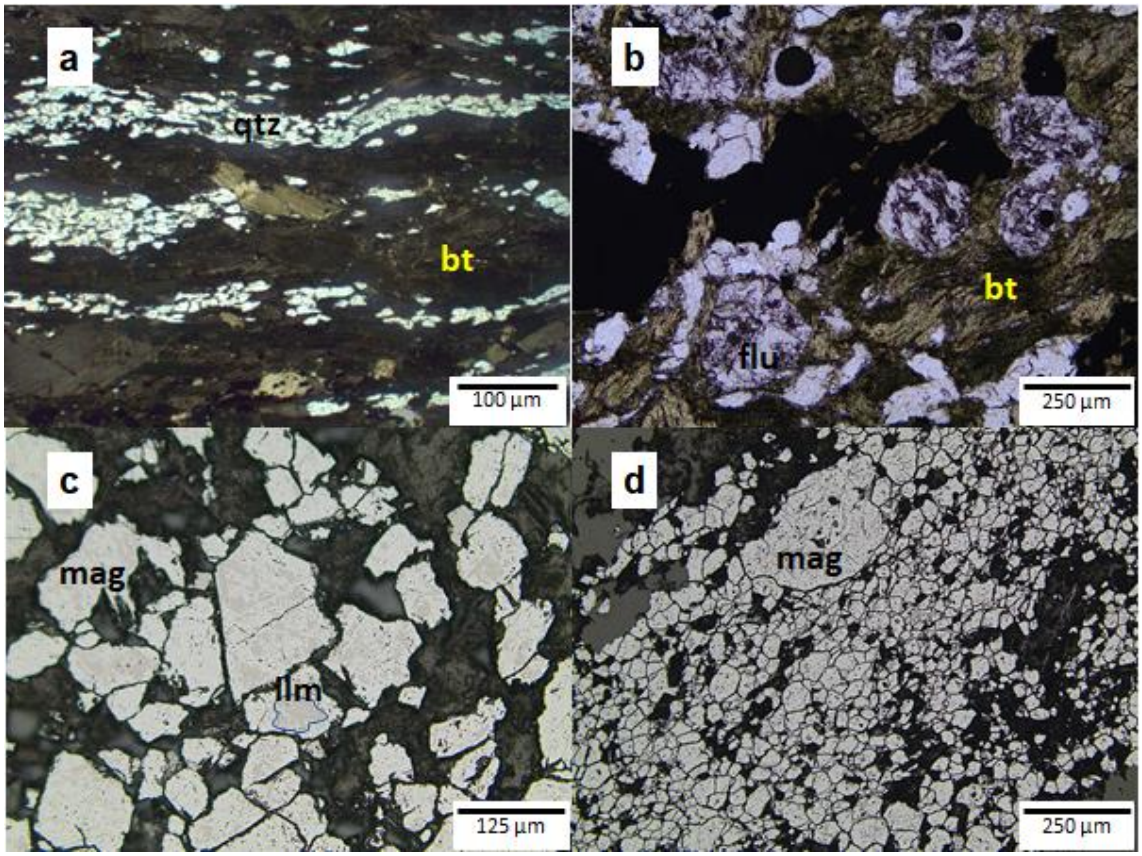

Figure 9 - Polished thin sections of garnet-biotite schist observed under refracted and transmitted light. a) Biotite-rich and quartz-rich alternating bands that form the rock schistosity (P//); b) Detail of fluorite (purple), biotite and opaque minerals (P//); c) Detail of magnetite grains with ilmenite exsolution textures. D) Granoblastic magnetite and ilmenite filling fractures in coarse-grained garnet. bt = biotite; flu = fluorite; ilm = ilmenite; mag = magnetite; qtz = quartz.

granoblastic magnetite (Figure 9d) that has ilmenite exsolutions (Figure 9c) and bornite and chalcocite inclusions.

Magnetite schist

Dark colored magnetite schist is formed of fine-grained foliated magnetite that is cut by late forming light-colored calcite, fluorite, quartz, chlorite and bornite veins (figure 3c).

Magnetite schists are made of >80% magnetite with minor biotite, apatite, quartz and altered garnet. Granoblastic texture and tectonic foliation (10a) are cut by at least two directions of brittle veins containing fluorite, calcite, bornite, chalcocite, digenite, chalcopyrite, chlorite, Fe-pyrosmalite, and quartz (Figure 10c, 10d and figure 11a). Bornite, chalcocite, and digenite fill interstices between phyllosilicates lamellae (Figure 11c) and magnetite grains, fractures and veins (Figure 10 and figure 11). Magnetite, chalcocite and digenite present symplectitic texture (10b and 10c), denoting the exsolution of the lower T phases (Digenite-Chalcocite) from a bornite solid solution. Chalcopyrite only appears as accessory in few samples. Molybdenite and graphite are sometimes folded, usually occur following the foliation and are more abundant closer to veins

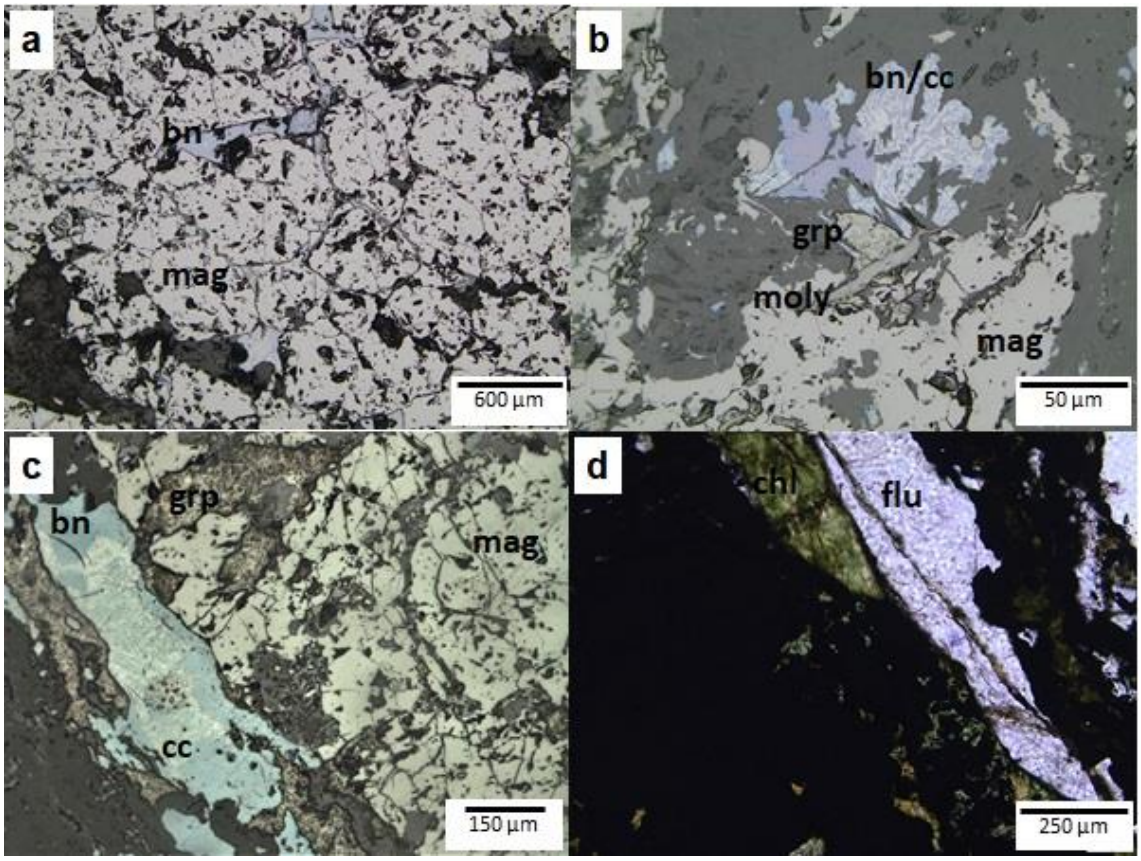

Figure 10 - Polished thin sections of magnetite schist observed under reflected (a, b, c) and refracted (d, P//); a) Granoblastic texture in very fracture magnetite, where interstices and fractures are filled with bornite and chalcocite. Some dispersed graphite lamellae. b) Bornite and chalcocite symplectitic texture. Graphite and molybdenite lamellae at the center of the photo. c) Bornite and chalcocite with symplectitic texture that are associated to graphite filling a vein. Very fractured magnetite. d) Fluorite, bornite (opaque mineral) and chlorite vein.

(10c and 11b). Chalcopyrite and uraninite inclusions were observed in magnetite. Fractured grains of ETR-rich minerals were observed in SEM images (Figure 11b). Magnetite presents granoblastic texture.

Mineral chemistry

Gangue minerals

Apatite

Apatites analyzed come from chalcopyrite breccia and magnetite breccia. The analyzed apatites classify as fluorapatites with F contents between 3.6 and 5.1 wt% F, and very low chlorine vs fluorine content ratio, with $X_{Cl}/X_F < 0.012$. There is also a somewhat higher substitution of Ca by Fe, with Fe content varying between 0.08 and 0.4 wt%.

Fayalite

Olivine grains are associated with magnetite breccia containing grunerite and ferrossilite clasts in a magnetite matrix. Grains can be very altered to chlorite but always retain the granular habit and high relief. Chemical compositions of olivine indicate an Mg:Fe ratio of 0.02 to 0.03 which

corresponds to an almost pure fayalite end member. There is also some substitution of Mg/Fe by Mn in the samples (0.6 – 1.1 MnO wt%). Significant F content of up to 1.4 wt% was also observed.

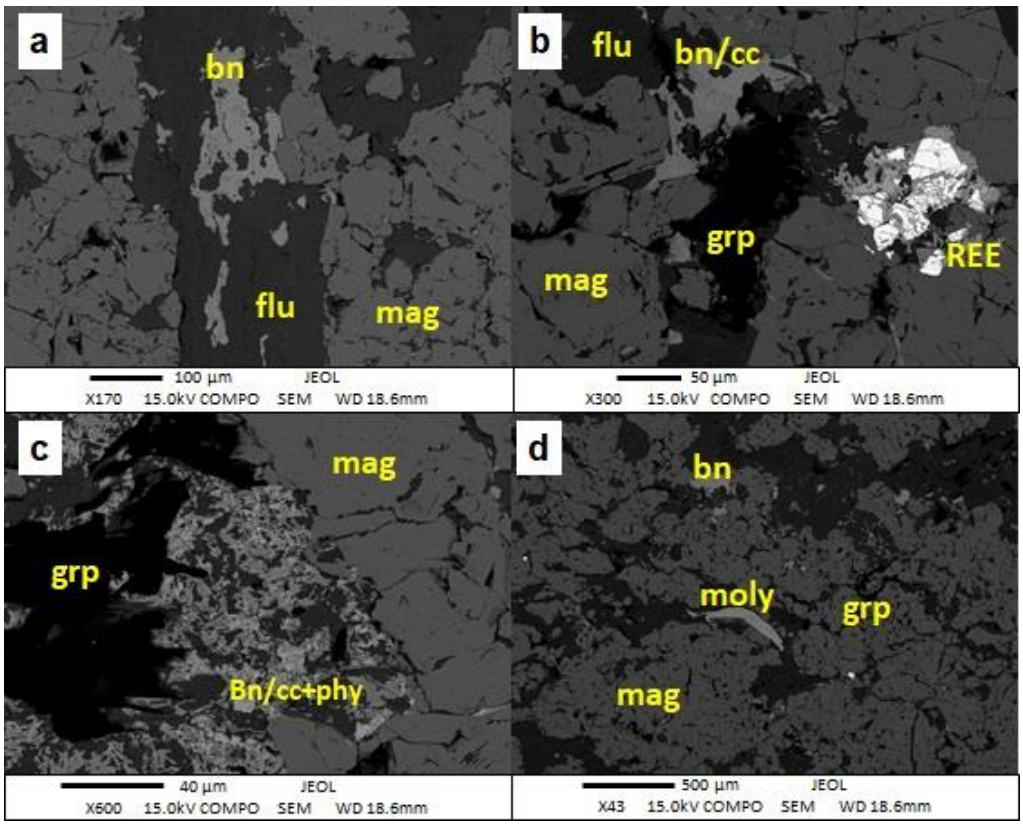

Figure 11 - Scanning electron microscope images of polished thin sections with carbon coating produced on BSE mode. a) Fluorite and bornite vein cutting granoblastic magnetite. b) Fractured REE-rich mineral with bornite-chalcocite-phyllosilicates association occupying the open spaces. Fluorite vein with bornite and graphite cutting through magnetite. c) Bornite-chalcocite and fine phyllosilicates association around graphite (black) at the left of the image and magnetite at the right portion. d) Folded molybdenite lamelle at the center of the image. Some scattered graphite (black), bornite (light gray), silicates (dark gray) and uraninite (white points) between magnetite (medium gray) grains.

Ferrossilite

Magnetite breccia samples were the only to provide pyroxene identification, however the minerals are rare, fine-grained, altered and usually associated to magnetite and grunerite presence. The cleavage planes were not always visible and the dark brown color was sometimes difficult to distinguish in between the opaque minerals. Analytical totals of the three points analyzed in pyroxenes close at 99 wt%. The data demonstrated that the mineral has closer affinity to the ferrossilite solid solution end member than enstatite, with Wo<2.5, Ens < 23.5 and Fs >75. Fluorine varies between 0.14 and 0.4 wt%F, 0.1 to 0.2 wt%Cl and 0.3 to 0.4 wt%Mn.

Amphibole (Fe-Actinolite, Grunerite, Hastingsite and Ferro-ferri-hornblende)

Analyzed amphiboles appear as clasts in chalcopyrite breccia and their analyses were necessary in order to better identify the three different species distinguished in thin section microscopy. Those species are: (1) strongly pleochroic dark green to yellowish green amphibole with little to no secondary alterations, mostly tabular in habit but may also substitute other amphiboles; (2)

amphibole with weak pleochroism in tones of light yellow to light green, rarely twinned, usually with alterations along the cleavage and at the center of anedral to subhedral (elongated tabular habit) crystals; and (3) amphibole with pleochroism from brown to light brown, frequently twinned, anedral crystals.

A table with calculated chemical formulas on 24 (O-Cl-F) basis and for a representative set of compositions is provided below (Table). Using Locock (2014) classification spreadsheet to calculate de chemical formulas, the three different amphibole types were identified (Figure 12, Figure 13 and Figure 14; from Leake et al., 1997) as: (1) hornblende, (2) Fe-actinolite and (3) grunerite. The most common amphibole is Fe-actinolite, with grunerite being the less abundant and appearing mainly in magnetite-rich samples of the breccia.

Table 2 - Table with representative amphibole analyses and their calculated chemical formula com the basis of 24 (O, Cl, F) as indicated by Locock (2014)

wt%	**Fe-Actinolita**		**Grunerita**		**Ferro-Ferri-Hornblenda**		**Hastingsita**	
SiO2	50,966	50,303	49,143	44,506	44,74	45,328	42,229	43,175
TiO2	0	0,2	0	0,101	0,026	0,046	0,219	0,15
Al2O3	0,349	0,322	1,114	3,715	6,086	5,041	7,917	8,116
V2O3	0	0,035	0	0	0,04	0,083	0	0
FeO	29,04	30,527	37,402	36,564	30,385	31,191	31,208	30,034
MnO	0,318	0,367	0,386	0,333	0,174	0,186	0,158	0,234
MgO	4,882	4,78	6,575	5,529	4,252	4,603	3,376	3,799
BaO	0,1	0	0	0,137	0	0,02	0	0,058
CaO	11,611	12,282	2,042	4,387	10,377	10,067	10,435	10,656
Na2O	0,06	0,036	0,356	0,917	1,58	1,256	1,786	1,733
K2O	0,007	0,021	0,074	0,355	0,439	0,237	0,779	0,521
Cr2O3	0	0,012	0,114	0,041	0	0	0	0
NiO	0,032	0	0,03	0,032	0,038	0	0	0
P2O5	0	0,088	0	0,034	0,009	0	0	0,059
F	0,007	0,023	0,129	0	0,277	0,277	0,341	0,229
Cl	0,054	0,028	0,197	1,025	0,936	0,734	1,342	1,496
Total	97,411	99,008	97,464	97,445	99,031	98,786	99,343	99,826
Fórmula química calculada com base em 24 (O,F,Cl)								
TSi	7,979	7,776	7,799	7,123	7,056	6,771	6,671	6,745
TP		0,006		0,002		0,001		0,004
TAl	0,021	0,059	0,201	0,701	0,925	1,228	1,329	1,251
TTi		0,023		0,012	0,005			
TFe3+		0,136		0,161	0,013			
CTi						0,012	0,026	0,018
CAl	0,043		0,008			0,073	0,145	0,244
CV		0,004			0,01			
CCr		0,001	0,014	0,005		0,005		
CFe3+		0,168	0,165	0,779	0,842	0,669	0,677	0,569
CNi	0,004		0,004	0,004				
CMn2+	0,011	0,048						
CFe2+	3,802	3,642	3,254	2,892	3,08	3,367	3,357	3,285
CMg	1,139	1,102	1,556	1,319	1,068	0,873	0,795	0,885
BMn2+	0,031		0,052	0,045	0,025	0,011	0,021	0,031
BFe2+			1,546	1,062	0,126	0,065	0,088	0,07
BCa	1,948	2	0,347	0,752	1,679	1,838	1,766	1,784
BNa	0,018		0,055	0,141	0,17	0,087	0,124	0,115
ACa		0,034						
ANa		0,011	0,054	0,144	0,209	0,408	0,423	0,41
AK	0,001	0,004	0,015	0,072	0,047	0,133	0,157	0,104
Sum T,C,B,A	14,997	15,014	15,07	15,214	15,255	15,541	15,579	15,515
OH	1,982	1,981	1,882	1,722	1,67	1,489	1,47	1,491
F	0,003	0,011	0,065		0,136	0,186	0,17	0,113
Cl	0,014	0,007	0,053	0,278	0,194	0,325	0,359	0,396
Mg/(Mg+Fe)	0,23052	0,232293	0,323493	0,31323	0,257473	0,205896226	0,191474	0,21223

Hornblende compositions can be further divided into hastingsite, ferro-ferri-hornblende and only one analysis being classified as ferro-edenite (Figure 12 and Figure 13), though no petrographic difference was noticed between them. Hastingsite has lower #Mg (0.13-0.2) than ferro-ferri-hornblende (0.2 <#Mg< 0.33). Ferro-ferri-hornblende has lower Al^{IV} content, typically 0.7 to 1.3, than hastingsite (1.1 to 1.6). Values of $0.2 < (Na+K)_A < 0.5$ are typical of ferro-ferri hornblende, while hastingsite has $0.5 < (Na+K)_A < 0.8$. Ferro-ferri-hornblende has up to 0.4 wt%F and between 0.6 < Cl <1.4 wt%Cl while hastingsite contents of fluorine 0.06 < F < 0.43 wt% F which

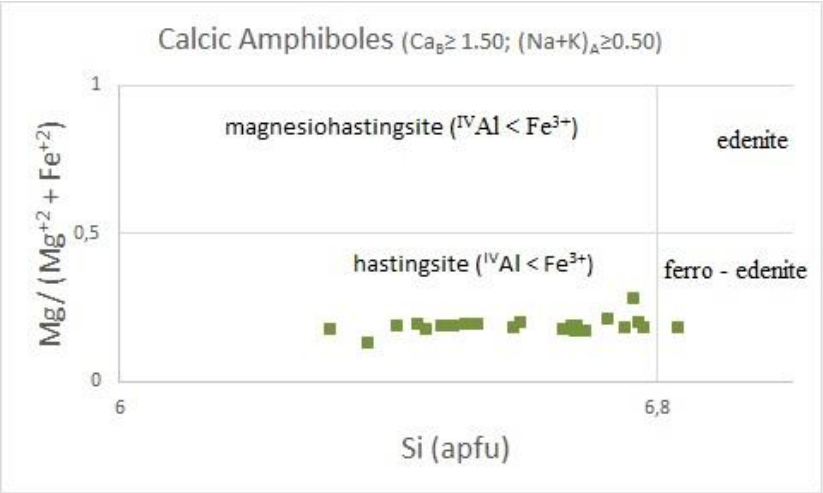

Figure 12 - Distribution of analytical points obtained for calcic amphiboles with (Na + Ca)$_A$ >0.5 a on diagram from Leake et al. (1997)

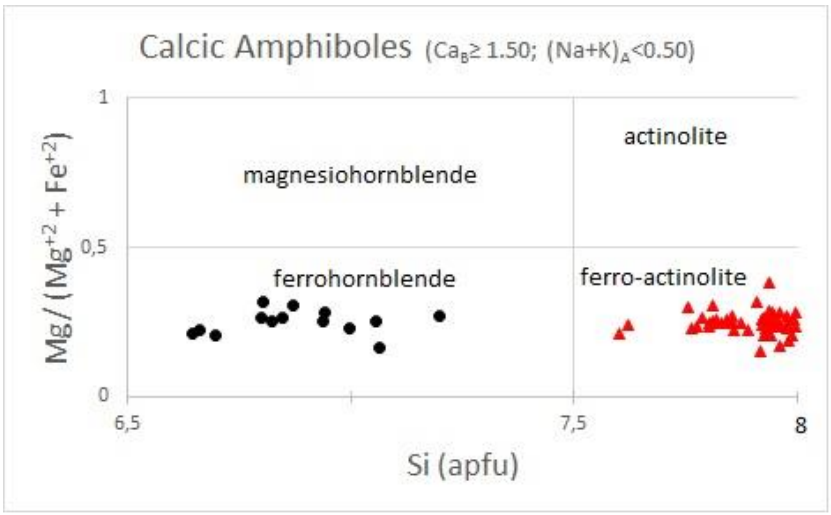

Figure 13 - Distribution of analytical points obtained for calcic amphiboles with (Na + Ca)$_A$ <0.5 a on diagram from Leake et al. (1997)

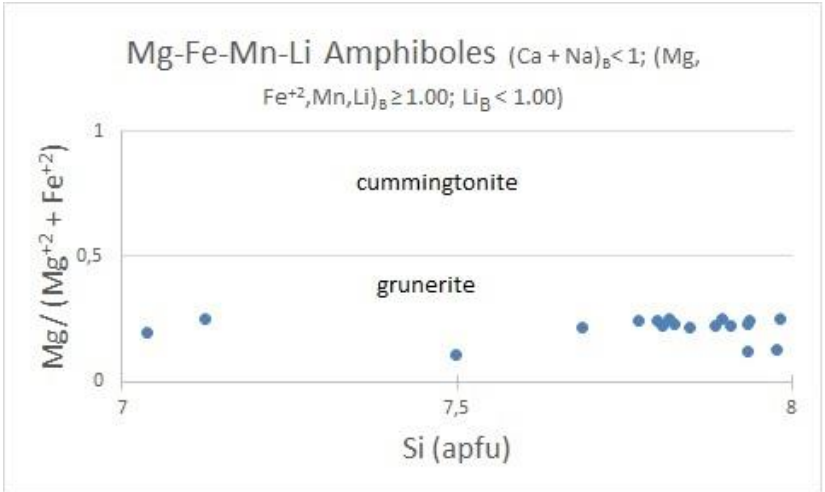

Figure 14 - Distribution of analytical points obtained for Fe-Mg amphiboles on diagram modified from Leake et al. (1997)

is similar to the content ferro-ferri-hornblende, and chlorine varies from 0.9 to 2.75 wt%Cl, the highest of all of the amphibole analyses. Fe-actinolite #Mg has a slightly higher range, 0.15-0.38,

than that of hornblendes and grunerite. It also has significantly lower Al^{IV} content (Al^{IV}<0.2) and $(Na+K)_A$ sums, which are >0.05. Contents of fluorine in Fe-actinolite goes up to 0.14wt%F and up to 0.21wt%Cl, which is the lowest of the amphiboles. Grunerite has a similar #Mg of that found for hornblende, when considered both varieties, ranging from 0.15 to 0.33. Grunerite also has the lowest Al^{IV} content (Al^{IV}< 0.09) than all the other amphiboles and $(Na+K)_A$ <0.22. Grunerite has between 0.11 <Cl <1.02 wt%Cl and up to 0.4wt% F.

Ore minerals

Representative analyses of ore minerals are shown in **Erro! Fonte de referência não encontrada.**. Ternary graphs of ore minerals include data obtained by Fernandez (2002) when characterizing the Salobo ore to enable copper concentration for the start of the Salobo Mine production. This data was used for result comparisons.

Cu-Fe sulfides – Chalcopyrite, Bornite, chalcocite

Chemical analyses of chalcopyrite were made both in the chalcopyrite matrix of the hydrothermal breccia and in smaller interstice-filling chalcopyrite of less mineralized samples. Chalcopyrite has a composition close to the ideal (Figure 16a). It also has up to 0.2 wt% of Zn, 0.1 wt% of Se, 0.3 wt% of Pb, 0.14 wt% of Bi, 0.1 wt% of Co, and 0.2 wt% of Mo. In some crystals it can also have high gold and silver contents, with up to 1.1 wt% of Au and 0.2 wt% of Ag.

Since bornite and chalcocite occur in a very fine symplectitic texture, some of the analyses probably represent an intermediate composition between the two of them. Other than chalcocite and bornite, digenite was also identified (Figure 15), and is another phase derived from the bornite solid solution at low temperatures, just as chalcocite. The compositions vary within the end members of the solid solution and go from 81.4 wt% Cu at the chalcocite end member to 57 wt% Cu at the bornite end member. Iron content goes from zero in chalcocite to as high as 16 wt% Fe in the bornite end member. The compositions closer to chalcocite end-member contain an average of 529 ppm of silver, while bornite has an average of 396 ppm Ag and digenite 305 ppm of Ag. When considering all analyses, including intermediate compositions, variation goes up to 1880ppm.

Bismuth values range from 1790 to 0 ppm for bornite and 1300 to 0 ppm for chalcocite. Gold contents can be relatively high in bornite since some crystals that contain values as high as 600 ppm of the metal. Peak values of gold on chalcocite are lower (up to 440 ppm). Concentrations of cobalt are higher than zero in most of the data of both chalcocite and bornite end members, reaching 460 ppm. However, cobalt is preferentially incorporated to bornite and then chalcocite. Selenium contents in chalcocite rage from 0 to 970 ppm and is chiefly higher in bornite (up to 1390 ppm), which may also indicate a preferential incorporation of selenium by bornite.

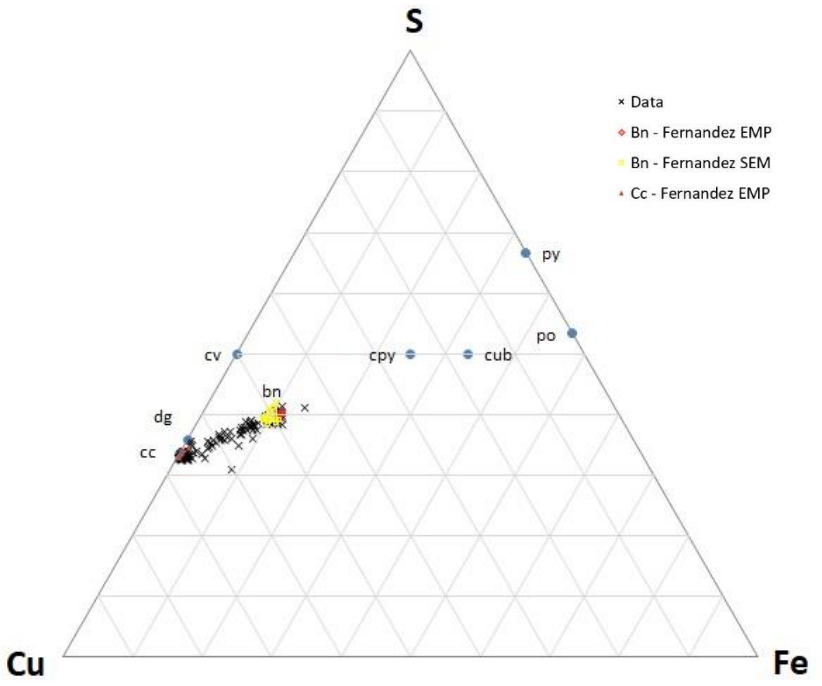

Figure 15 -Bornite, digenite and chalcocite compositions distribution along intermediate composition between these minerals.

Fe-Ni sulfides

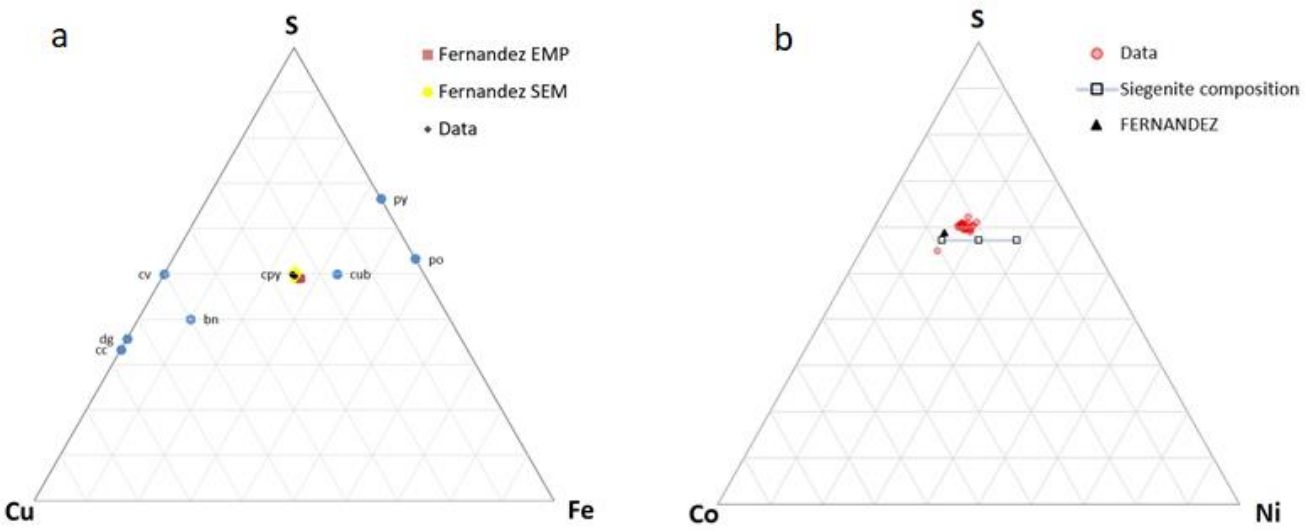

Figure 16 - Ternary graphs for chalcopyrite (a) and siegenite compositions.

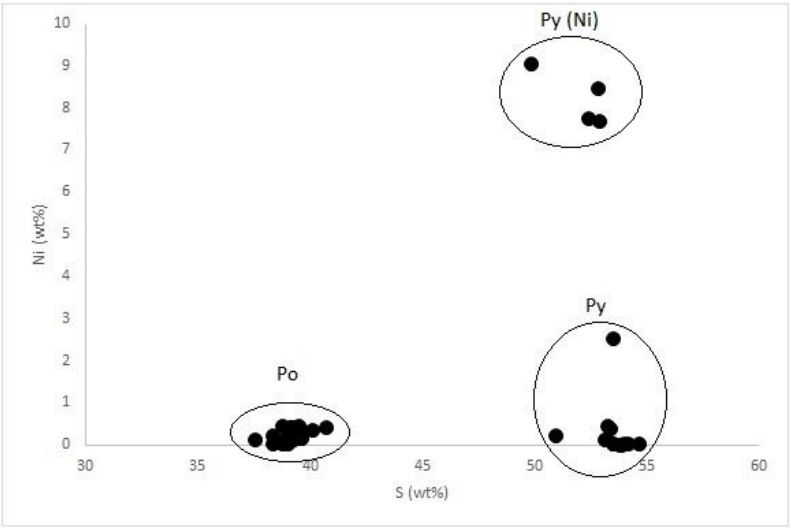

Figure 17 - Pyrite and pyrrhotite on a plot of nickel vs sulfur content and highlighted compositions of each mineral population

Pyrite crystals also have different color domains, that have slightly grayer color, described in optical microscopy. Plotting their sulfur *vs* nickel content (in weight percentage) it is possible to distinguish the two different compositions of these contrasting pyrite domains (Figure 17). Therefore, a content of 7.69 to 9.04 wt% of nickel for the grayer zones are greater than those obtained for the rest of the crystal with a range of 0 to 0.44 wt% of nickel. This implies the existence of nickel-rich domains in pyrite grains. The Ni-rich pyrite crystal zones are much farther to that of an ideal pyrite composition than the rest of the analyses. Pyrite has some copper incorporation of up to 0.23 wt% for both domains.

Pyrrhotite can be a product of pyrite reaction or appear as anedral light pink crystals formed between chalcopyrite matrix and Fe-minerals clasts, such as magnetite and amphiboles. Due to

crystal size restrictions only the second of the cited was analyzed. Pyrrhotite has lower sulfur contents than pyrite. However, analyses of Salobo pyrrhotites showed that they may contain up to 0.46 wt% of Ni and up to 0.26 wt% of Co. It also has up to 0.30 wt% of Pb and 0.12 wt% of Co.

Siegenite is a cobalt and nickel sulfide that also has significant amount of iron and sometimes copper $(Co, Ni)_3S_4$. It is commonly associated with chalcopyrite and has an intermediate composition between the polydymite ($NiNi_2S_4$) and linnaeite ($CoCo_2S_4$) end members (10b). Only hydrothermal amphibole breccias contain this ore mineral, which is commonly associated to pyrrhotite in chalcopyrite matrix. There is a wide distribution on Fe and Cu amounts, with 0.4 to 17 wt% and up to 9.5 wt%, respectively. The upper limits for copper and iron content in the samples are greater than the expected for siegenite and may represent an interference of chalcopyrite due to matrix effect on the analysis results. Sulfur contents at Salobo siegenite are a little higher than the ideal formula range (Figure 16b).

Accessory-to-trace ore minerals

Selected representative analyses are shown in Table 3.

Both analyses of gold had high Ag contents, around 13 wt%. Contents of Cu (0.6-0.7 wt%) and Fe (0.3-0.4 wt%) are also relatively high. Molybdenite has high Bi (0.1 – 0.2 wt%) and Au (0.5 wt%). Galena has significant amounts of Fe (1.6 wt%), Cd (0.15 wt%), Se (0.25 wt%) and Cu (0.4 wt%). Finally, sphalerite has 56 wt% of Zn and 11.4 wt% of Fe, as well as trace amounts of cobalt (0.4 wt%) and Se (0.1 wt%) and Pb (0.1 wt%).

Table 3 - Representative ponctual EPMA analyses of ore minerals (wt%).

As	Zn	Ga	Se	S	Pb	Bi	Cd	Te	Fe	Co	Cu	Ni	Sn	Sb	Ag	Pd	Mo	Au	Pt	Total	Mineral
0,00	0,04	0,00	0,03	24,71	0,07	0,11	0,00	0,00	11,38	0,04	64,21	0,02	0,01	0,00	0,06	0,00	0,07	0,00	0,00	100,73	Bornite
0,00	0,09	0,00	0,06	24,75	0,03	0,00	0,00	0,00	10,43	0,02	64,17	0,00	0,02	0,00	0,08	0,00	0,01	0,00	0,00	99,65	Bornite
0,00	0,00	0,00	0,00	20,59	0,03	0,00	0,00	0,00	0,31	0,00	79,31	0,00	0,02	0,00	0,07	0,00	0,00	0,00	0,00	100,34	Calcocita
0,00	0,00	0,00	0,00	20,45	0,11	0,00	0,00	0,00	1,05	0,00	77,71	0,02	0,07	0,01	0,19	0,00	0,00	0,01	0,00	99,61	Chalcocite
0,00	0,16	0,00	0,02	21,81	0,09	0,02	0,00	0,00	3,91	0,00	74,70	0,00	0,00	0,00	0,07	0,00	0,03	0,00	0,00	100,81	Chalcocite/Bornite
0,00	0,20	0,00	0,10	24,08	0,14	0,11	0,00	0,01	8,57	0,00	67,41	0,00	0,03	0,00	0,03	0,00	0,10	0,01	0,00	100,79	Chalcocite/Bornite
0,00	0,04	0,00	0,09	21,47	0,00	0,02	0,00	0,00	4,03	0,02	76,71	0,00	0,01	0,00	0,03	0,00	0,03	0,03	0,00	102,46	Digenite
0,00	0,13	0,00	0,02	21,60	0,14	0,00	0,00	0,00	3,86	0,00	76,25	0,00	0,00	0,00	0,04	0,00	0,09	0,00	0,00	102,12	Digenite
0,00	0,04	0,00	0,02	34,62	0,16	0,08	0,01	0,04	30,75	0,00	34,74	0,00	0,00	0,00	0,00	0,00	0,09	0,00	0,00	100,54	Chalcopyrite
0,00	0,00	0,00	0,04	34,51	0,12	0,00	0,00	0,00	30,76	0,03	34,72	0,00	0,00	0,00	0,03	0,00	0,05	0,01	0,00	100,27	Chalcopyrite
0,00	0,00	0,00	0,01	39,54	0,22	0,00	0,02	0,00	59,54	0,10	0,20	0,14	0,06	0,00	0,00	0,00	0,00	0,00	0,00	99,83	Pyrrhotite
0,00	0,03	0,00	0,02	39,50	0,16	0,00	0,04	0,00	59,35	0,10	0,18	0,21	0,00	0,00	0,00	0,00	0,10	0,00	0,00	99,69	Pyrrhotite
0,00	0,03	0,00	0,08	50,92	0,28	0,00	0,07	0,02	46,91	0,10	0,14	0,22	0,00	0,02	0,00	0,00	0,17	0,00	0,00	98,96	Pyrite
0,00	0,04	0,00	0,03	53,27	0,25	0,00	0,03	0,00	46,67	0,09	0,00	0,44	0,00	0,00	0,00	0,00	0,08	0,00	0,00	100,89	Pyrite
0,01	0,01	0,00	0,08	53,51	0,30	0,00	0,03	0,03	45,97	0,27	0,00	2,53	0,00	0,00	0,02	0,00	0,09	0,00	0,00	102,85	Ni-rich pyrite
0,00	0,02	0,00	0,00	41,73	0,13	0,00	0,00	0,11	17,07	19,71	0,00	18,49	0,00	0,00	0,00	0,01	0,10	0,00	0,00	97,36	Siegenite
0,00	0,00	0,00	0,01	41,57	0,16	0,00	0,00	0,13	11,87	20,97	1,12	20,57	0,04	0,00	0,00	0,00	0,07	0,00	0,00	96,51	Siegenite
0,00	0,00	0,00	0,02	0,31	0,00	0,00	0,12	0,00	0,36	0,04	0,73	0,00	0,00	0,00	13,20	0,00	0,07	86,33	0,00	101,17	Gold
0,00	0,04	0,00	0,04	0,16	0,00	0,00	0,00	0,03	0,28	0,03	0,58	0,02	0,00	0,00	12,77	0,00	0,03	86,53	0,00	100,49	Gold
0,03	0,02	0,00	0,00	41,77	0,00	0,13	0,02	0,00	0,24	0,00	0,07	0,01	0,00	0,02	0,02	0,00	59,17	0,51	0,00	102,00	Molybdenite
0,00	0,01	0,00	0,00	41,70	0,00	0,31	0,00	0,00	0,09	0,00	0,03	0,04	0,00	0,00	0,00	0,00	58,98	0,49	0,00	101,65	Molybdenite
0,00	0,04	0,00	0,25	13,34	86,83	0,00	0,15	0,04	1,63	0,00	0,36	0,00	0,02	0,00	0,00	0,00	0,06	0,00	0,00	102,73	Galena
0,00	55,88	0,00	0,13	32,96	0,12	0,00	0,06		11,36	0,36	0,03	0,00	0,00	0,00	0,00	0,00	0,11	0,00	0,00	101,00	Sphalerite

Discussion

Cu-Fe sulfides and ore-formation conditions

The most abundant ore mineral of the two breccias is chalcopyrite. This means that the mineralization processes occurred mainly in the Fe-Cu-S system, but crystallization of siegenite, traces of Co-pentlandite and the presence of zones of high nickel content in pyrite demonstrate Ni and Co enrichment of the sulfide-rich fluid that originated the ore.

Chalcopyrite composition is located in the central portion of the Fe-Cu-S system ternary diagram (Figure 18) and constitutes a large solid solution field (iss) at high temperatures. This solid solution field begins to shrink under 700ºC but retains tie lines to the bornite solid solution at the Cu-rich end of the system (Cabri, 1973; Cook et al., 2011; Yund and Kullerud, 1966). Pyrite and pyrrhotite presence can be a result of phase separation within the iss solid solution field, but the fact that pyrrhotite concentrates between clasts and chalcopyrite contacts suggests that it was formed as a product of redox reaction caused by the interaction of the Fe-rich, previously formed mineral phases and the sulfide-rich fluid. Traces of bornite as inclusions in magnetite clasts, in

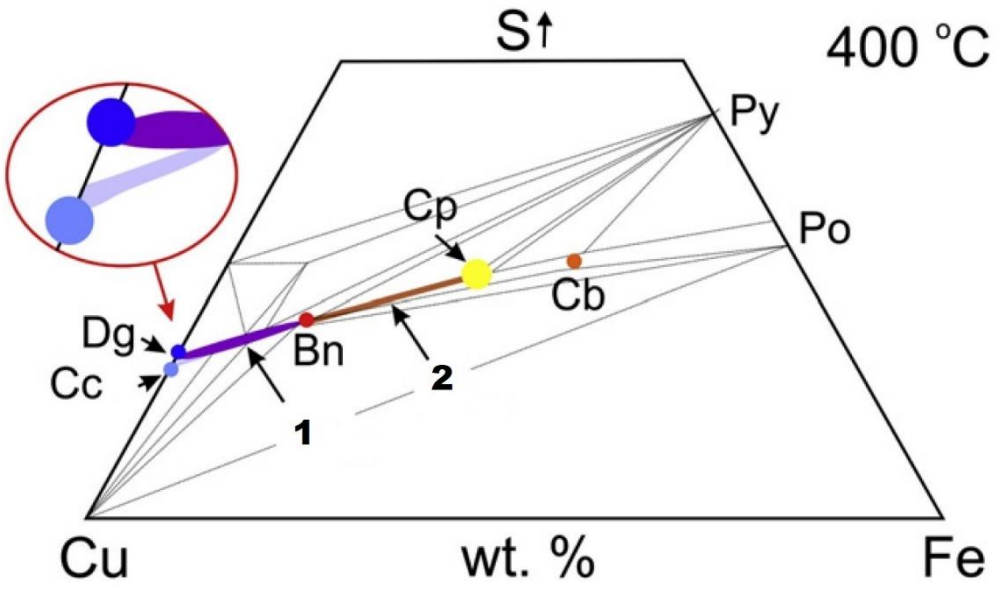

Figure 18 – Representation of the Fe-Cu-S system showing (1) bornite solid solution and (2) chalcocite solid solution (icc) fields (modified from Ciobanu et al., 2017)

equilibrium with chalcopyrite, can also be explained by high temperature phase separation, however supergenic processes where chalcopyrite tends to loses iron and acquire more Cu-rich compositions cannot be discarded (Ciobanu et al., 2017; Craig and Vaughan, 1990). In addition, the high contents of nickel on some pyrite crystals were probably incorporated at high temperatures and formed zones of Ni-pyrite within the crystals as cooling diminished the nickel incorporation capacity.

In these conditions, bornite and chalcopyrite found in clasts of amphiboles of the breccias and in hydrothermally altered granitic rock would be the earliest observed Cu-Fe sulfides be formed and their coexistence might be due to either high-temperature phase separation or Cu-enrichment supergenic processes. This early Cu-Fe sulfide formation is limited if compared to the following formation of chalcopyrite that occurred as the chalcopyrite breccia formed and chalcopyrite crystallized as its matrix. Within the chalcopyrite matrix pyrite and pyrrhotite could also be a result of high-temperature phase separation, however that doesn't seem to be the case for pyrrhotite, that appears to have been formed after contact reactions between clasts and the matrix.

Finally, most of the deposit's bornite is found in magnetite schists, normally on veins and showing a symplectitic texture in association to chalcocite that formed late when compared to previously described Cu-Fe sulfide formation. Bornite and chalcocite are part of the copper-rich portion of the Fe-Cu-S system. The copper-rich portion of the Fe-Cu-S system is complex: many phases form at low temperatures and includes a large solid solution field that includes bornite and chalcocite compositions (bornite solid solution, or bss) at high temperatures. This wide solid solution field separates when chalcocite crystallizes, below 435 °C. After this point, most of the solid solution field will correspond to a bornite-digenite solid solution and only a smaller portion will have bornite-chalcocite end members (Cabri, 1973; Chakrabarti and Laugghlin, 1983; Craig and Scott, 1974; Yund and Kullerud, 1966). The bss fields shrinks as cooling proceeds and from this process results the appearance of intergrowths and exsolutions, including symplectitic texture from the studied samples under 335 °C (Craig and Scott, 1974; Requia, 1995). If chalcocite and digenite are in equilibrium, that would indicate a possible temperature range of 435°C to 93 °C (Chakrabarti and Laugghlin, 1983; Roseboom Jr, 1966) giving a lower limit for the paragenesis. However, it is hard to be certain of the equilibrium since there are few digenite grains, and they could also be formed by supergenic processes.

Another evidence for low temperature crystallization of ore minerals in the magnetite schist is their association with fluorite, calcite, pyrosmalite and graphite. Thus, formation of a bornite-rich ore from a thermal-induced remobilization of chalcopyrite-rich primary ore can be explained by the loss of iron during hydrothermal event from chalcopyrite chemistry and consequently assume more copper-rich compositions (Ciobanu et al., 2017; Craig and Vaughan, 1990). Thus, the Salobo bornite "high-grade ore" do not represent a shallower environment for the IOCG formation, as is the case in the Olympic Dam Complex, nor is a supergenic processes.

Metamorphism

Effective and extensive metamorphic remobilization of ore minerals requires liquid- or mixed-state (concurrent solid- and liquid-state transfer) mass transfer through variable amounts of fluids from multiple possible sources (Marshall et al., 1998). The fluid interacts with the primary ore using dynamic microfracture networks or transient and channelized flow through vein arrays that

are commonly related to shear zones (Marshall et al., 1998). Guides to fluid-induced transfer include: (1) more simple fracture fill sulfide mineralogy than in the primary body; (2) gangue phases intergrows with sulfide filling fractures and (3) fracture fill minerals that are different from those recorded in the source (Marshall et al., 1998).

The Salobo high grade ore is characterized by extensive bornite and chalcocite in fluorine-chlorite-calcite-quartz brittle veins that crosscut the preexisting tectonic foliation in the magnetite schist. Vein minerals indicate that the precipitation of the ore occurred from a F- and CO_2-rich fluid at low temperatures. The high-grade ore is located in a transcurrent fault system associated to the Cinzento Shear Zone and undulose extinction on recrystallized quartz crystals, granoblastic texture of magnetite and intense tectonic foliation indicates that deformation represent a pervasive recrystallization process within the magnetite schist. The ore mineralogy is mainly constituted of bornite and chalcocite, with little digenite and molybdenite, being substantially less complex than the breccia ore, which includes several mineral phases. Bornite and chalcocite are observed in intergrowth textures with phyllosilicates such as chlorite and Fe-pyrosmalite. Finally, fluorite and calcite, two of the most abundant vein filling minerals in the lithotype are rare in chalcopyrite breccia.

All the mentioned characteristics of the magnetite schist are compatible with a fluid-induced metamorphic remobilization of previously formed, higher temperature Cu-Fe sulfides, to form bornite-chalcocite veins.

Paragenetic associations and events sequence

From the mineralogical-textural observations it is possible to make some inferences regarding the paragenetic sequence of minerals at Salobo deposit (Figure 20). It is clear from the multiplicity of textures and morphologies, that there are more than one generation of magnetite and hematite, both of which are partly resulting of weathering processes and partly of result of hydrothermal fluids. The same happens for chalcopyrite, that appear as inclusions in minerals that formed prior to the chalcopyrite matrix formation. It's also possible to define the hydrothermal alterations and paragenetic mineral associations sequence.

Early hydrothermal minerals appear in the least altered granitic rocks, such as Na-scapolite and tourmaline, or as inclusions in other minerals, like chalcopyrite-bornite, uraninite and magnetite in amphibole crystals. Those minerals constitute an early-forming, incipient Na enrichment, that is mainly marked by Na-scapolite and tourmaline presence. Subsequent calcic-iron enrichment forms hornblende and Fe-actinolite, together with smaller amounts of ilvaite, apatite, allanite. In iron-rich portions, interpreted as representative of magnetitite bodies predating the sulfide ore, an assemblage of fayalite, ferrossilite and grunerite is formed, in addition to varying contents of the previously cited minerals and a decrease in chalcopyrite as a matrix content.

The occurrence of hydrothermal OPX in the Carajás Province, together with the association with Fayalite and Grunerite, require temperatures of more than 700 °C for the stabilization of such assemblage, as well as a fluid with low f_{H2O}. Such conditions are similar as those described in the GT-34 Ni-IOCG, located in the Southern Copper Belt (Garcia et al., submitted).

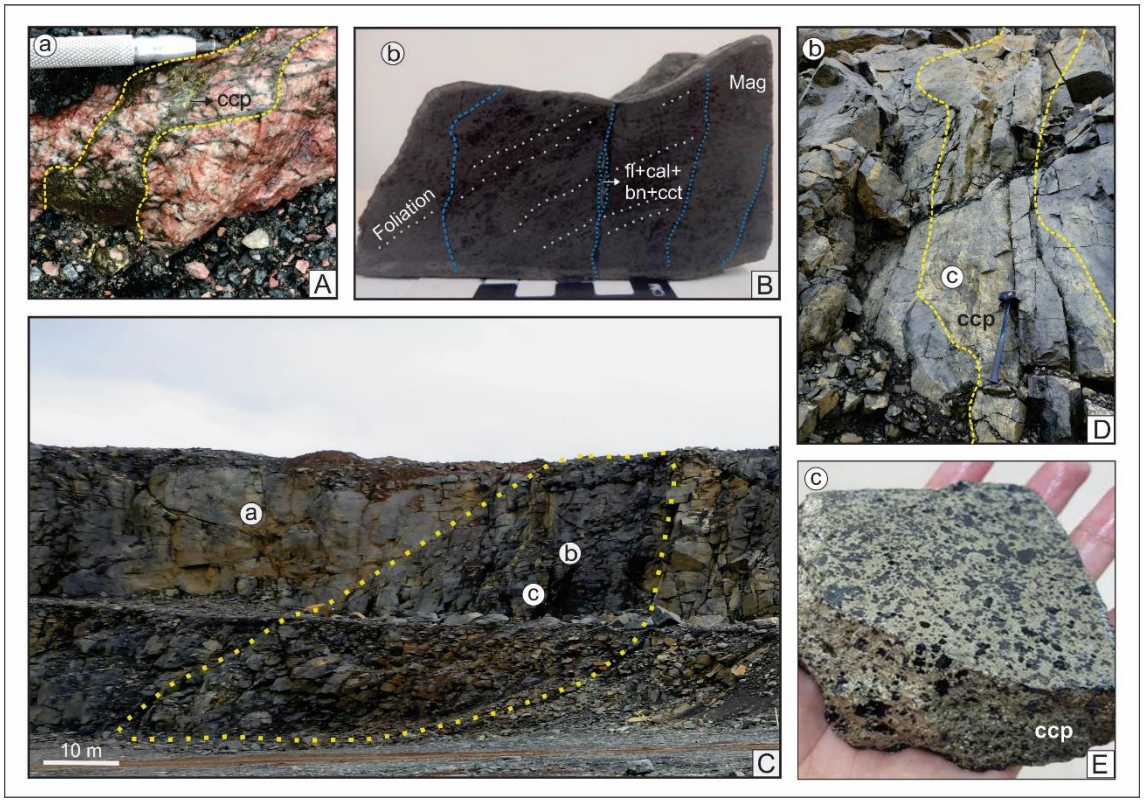

Figure 19 – A) Photo of granitic rock sample collected from (a), shown in photo C. The rock has chalcopyrite rich portions indicated in the photo by the yellow line. B) Magnetite schist collected from (b), shown in photo C. Tectonic foliation cut by fluorite, calcite, chalcocite and bornite veins are highlighted. C)View of the Salobo Mine open-pit where the hydrothermally granitic rocks, magnetite schist and chalcopyrite breccia samples were obtained. Corridor of intense deformation where magnetite schist was formed is marked by the yellow line. E) Chalcopyrite breccia with no macroscopically visible signs of deformation.

Following, sulfide-rich fluids produced brecciation, substitution along weakness planes and partially reacted with the existing minerals, forming a matrix with clasts locally involved by pyrrhotite. Ni, Co, Fe, Pb and Zn in excess in the sulfide fluid result in pyrite with nickel enriched portions, siegenite, pentlandite, pyrrhotite, magnetite, galena and sphalerite. This alteration sequence and primary mineralization event resumes the IOCG stage in the Salobo deposit and may have occurred around 2.73 Ga, the same age obtained for other IOCG deposits in the Carajás Province (Machado et al., 1991) and for the ore (Tassinari et al., 2003).

Afterwards, as the Cinzento Shear Zone reactivates around 2.55 Ga, garnet-biotite schist and magnetite schist form, coupled with a K-Si enrichment towards the rims of the Salobo mega-sigmoid, as well as intense magnetite recrystallization. Pressure shadows around garnet crystals indicate a syn-kinematic formation and an euhedral and free-of-inclusions outer rim overgrowing the foliation evidences a second-stage post-kinematic growth. Localized ilmenite lamellae that

occur in magnetite crystals represent exsolutions and may be interpreted as a result of cooling or as exsolution-oxidation processes. The hydrothermal altered granitic rock and the chalcopyrite breccia are only poorly preserved, as Q-domains within pressure shadows in corridors of intense deformation, now chiefly transformed to magnetite schists and garnet-biotite schists (Figure 19). That is caused by the fact that within the shear zone, some inflection planes generate portions of

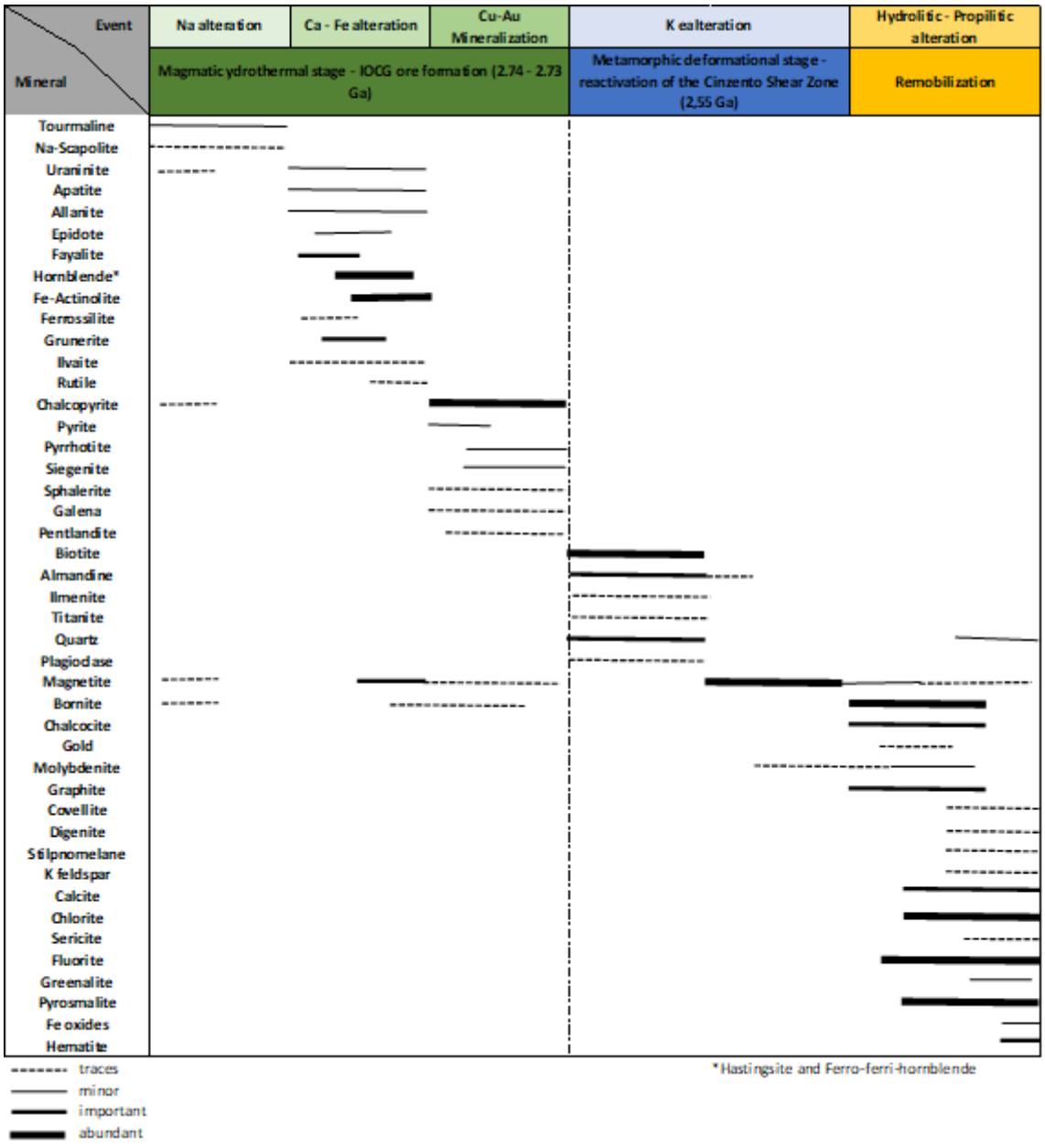

Figure 20 - Paragenetic sequence for Salobo deposit, including magmatic-hydrothermal alteration, metamorphic-deformational recrystallization and remobilization.

lower stress that are the least affected by relative movement. This allows the breccia to retain only minor deformation when compared to the adjacent rocks.

Melo (2014), when discussing the mineralization age pointed out that even though it has been suggested that the emplacement of the Old Salobo Granite, that has been dated as synchronic to the CSZ at 2.57 Ga, is the source of Cu-Au IOCG mineralization (Requia et al., 2003) the

alteration patterns of the granite and the ore are very different and suggests an older IOCG mineralization age of 2.76 Ga. In this case it would be possible that ages close to 2.55 Ga at the area represent a reset on isotopic system by an intense tectono-thermal event of CSZ reactivation that affected the molybdenite in the ore as well. Therefore, the crystallization and deformation of Igarape Gelado Suite, the activation of the CSZ, dynamic metamorphism and IOCG mineralization would be synchronic at 2.76 Ga and a posterior CSZ reactivation affected them at 2.55 Ga.

A stage younger than the metamorphic deformational stages promotes ore remobilization. This last event doesn't achieve temperatures as high as the others, as here described, resulting in the remobilization of the ore and the reequilibration of the previous assemblages at lower temperatures. Specifically regarding the Fe-Cu-S system, the symplectitic texture of bornite and chalcocite, associated with typically low-temperature minerals, such as graphite, calcite and fluorite, imply in a <335°C upper limit (Craig and Scott, 1974; Requia, 1995) for the recrystallization of the Salobo "high-grade ore". At this time, there is a formation of a particular assemblage, distinct from the typical IOCG (Pollard et al., 2018), including quartz-calcite-fluorite-phyllosilicates, which promotes Cu-Fe-sulfides remobilization. It also results in the hydration of previously formed silicates and oxidation towards hematite stability field.

It is possible that the remobilization occurred as a consequence of a 1.88 Ga event, age well-defined in the Carajás Province for the timing of voluminous A-type granitic magmatism. In this case sulfides would have been remobilized due to the emplacement and transport of lithophiles elements by a F- and CO_2-rich fluid.

Conclusions

In conclusion, the geological and metallogenetic history of the Salobo deposit is complex and have multiple superimposed hydrothermal alteration events and metamorphism along a major transcurrent shear zone, as well as association to granite intrusions. All of these factors resulted in a constantly changing bibliography about the deposit classification, metal sources, protoliths, host rocks and genesis. However, petrographic studies of different lithotypes and mineral chemistry when associated to the accumulated knowledge on the area make it possible to propose a new paragenetic/episode sequence that better explain the evolution of the deposit in relation to textures and mineralogy observed (Figure). Such evolution is characterized by one main Neoarchean primary mineralization event (2.73 Ga), where the IOCG stage took place.

In the IOCG formation context, an initial incipient Na-enrichment (Na-scapolite) evolves to a hydrothermal Ca-Fe enrichment (hornblende, Fe-actinolite, magnetite, apatite, ilvaite). The Fe enrichment in this stage also forms magnetitite bodies (that results in magnetite breccia) with ferrosilite, fayalite and grunerite. Subsequently, a sulfur-rich fluid promotes brecciation and the

deposition of the IOCG Cu-Fe sulfides, forming the chalcopyrite breccia. This sulfide fluid was also enriched in Co, Ni, Zn, Pb and Cu. Cooling of high temperature sulfide fluid promotes separation of phases of chalcopyrite solid solution generating pyrite and possibly bornite. Differentiation of Ni-rich zones within pyrite crystals is propelled by diminishing nickel incorporation capacity in pyrite crystals during cooling processes. Therefore, the main source ore concentration is a typical IOCG, characterized by a chalcopyrite-rich ore mineralization.

Reactivation of the Cinzento Shear Zone at c.a. 2.5 Ga affects the deposit rocks and results in a set of transcurrent faults, creating a vertical high-stress corridor where magnetite-rich rocks are transformed to a monotonous Mt-schist. Garnet-biotite schist are also formed towards the edges of the mega-sigmoidal structure, culminating in a mylonitic quartzite. The hydrothermally altered granitic rock and the chalcopyrite breccia are only preserved from high stress influence in the pressure-shadows and inflection planes.

Metamorphic remobilization of the source mineralization is driven by hydrothermal fluids of low temperature and high F and CO_2 from a later remobilization event, possibly, an extensive granite-related Cu-Au mineralization linked to a regional A-type magmatism (1.9 – 1.8 Ga). These fluids are channeled by the deposit's fault system and vein array under brittle conditions. Cooling of the precipitated vein-filling and Cu-Fe-rich sulfides of the bornite solid solution produces symplectitic textures of bornite and chalcocite.

References

Barros, C.E.M., Sardinha, A.S., Barbosa, J.P.O., Macambira, M.. J.B., 2009. Structure, petrology, geochemistry and zircon U/Pb and Pb/Pb geochronology of t e synkinematic Archean (2.7 Ga) A-type granites from the Carajás metallogenic province, northern Brazil. Can. Mineral. 47, 1423–1440.

Cabri, L.J., 1973. New Data on Phase Relations in the Cu-Fe-S S ystem. Econ. Geol. 68, 443–454.

Chakrabarti, D.J., Laugghlin, D.E., 1983. The Cu-S (Copper-Sulfur) System. Bull. Alloy Phase Diagr. 4 n^{o}3, 254–271.

Ciobanu, C.L., Cook, N.J., Ehrig, K., 2017. Ore minerals down to the nanoscale: Cu-(Fe)-sulphides from the iron oxide copper gold deposit at Olympic Dam, South Australia. Ore Geol. Rev. 81, 1218–1235.

Cook, N.J., Ciobanu, C.L., Danyushevsky, L.V., Gilbert, S., 2011. Minor and trace elements in bornite and associated Cu–(Fe)-sulfides: A LA-ICP-MS studyBornite mineral chemistry. Geochim. Cosmochim. Acta 75, 6473–6496. https://doi.org/10.1016/j.gca.2011.08.021

Craig, J.R., Scott, D., 1974. Sulfide Phase Equilibria, in: Sulfide Mineralogy, Sulfide Mineralogy. Reviews in Mineralogy, p. Chapter 5, CS-1-CS-110.

Craig, J.R., Vaughan, D.J., 1990. Compositional and textural variations of the major iron and base-metal sulphide minerals, in: Sulphide Deposits-Their Origin and

Processing. P.M.J. Gray, G.J. Bowyer, J.F Castle, D.J . Vaughan and N.A. Warner (eds). The Institution of Mining and Metallurgy, pp. 1–16.

de Freitas Toledo, P.I., Penteado Natividade Moreto, C., Xavier, R.P., Gao, J., da Silva Nogueira de Matos, J.H., de Melo, G.H.C., 2019. Multistage Evolution of the Neoarchean (ca. 2.7 Ga) Igarapé Cinzento (GT-46) Iron Oxide Copper-Gold Deposit, Cinzento Shear Zone, Carajás Province, Brazil. Econ. Geol. 114, 1–34. https://doi.org/10.5382/econgeo.2019.4617

DOCEGEO, 1988. Revisão litoestratigráfica da Província Mineral de Carajás - Litoestratigrafia e principais depósitos minerais.

Domingos, F.H.G., 2009. The structural setting of the Canaã dos Carajás region and Sossego-Sequeirinho deposits, Carajás, Brazil (Ph.D.). Durhan University, Durhan, United Kingdom.

Feio, G.R.L., Dall'Agnol, R., Dantas, E.L., Macambira, M.J.B., Gomes, A.C.B., Sardinha, A.S., Oliveira, D.C., Santos, R.D., Santos, P.A., 2012. Geochemistry, geochronology, and origin of the Neoarchean Planalto Granite suite, Carajás, Amazonian craton: A-type or hydrated charnockitic granites? Lithos 151, 57–73.

Feio, G.R.L., Dall'Agnol, R., Dantas, E.L., Macambira, M.J.B., Santos, J.O.S., Althoff, F.J., Soares, J.E.B., 2013. Archean granitoid magmatism in the Canaã dos Carajás area: implications for crustal evolution of the Carajás province, Amazonian craton, Brazil. Precambrian Res. 227, 157-.

Fernandez, O.J.C., 2002. Microquímica e mineralogia de processos do minério de cobre de Salobo, Carajás (Mestrado). Universidade Federal do Pará, Belém.

Ferreira Filho, C.F., Cançado, F., Correa, C., Macambira, E.M.B., Junqueira-Brod, T.C., Siepierski, L., 2007. Mineralizações estratiformes de PGENi associadas a complexos acamadados em Carajás: os exemplos de Luanga e Serra da Onça, in: Contribuições à Geologia Da Amazônia. Rosa Costa L. T., Klein E.L., Viglio E.P., SBG-Núcleo Norte, Belém, pp. 1–14.

Gibbs, A.K., Wirth, K.R., Hirata, W.K., Olszewski, W.J., 1986. Age and composition of the Grão Pará Group volcanics, Serra dos Carajás. Rev. Bras. Geociências 16, 201–211.

Grainger, C.J., Tallarico, F.H.B., Fletcher, I.R., 2008. Metallogenesis of the Carajás Mineral Province, Southern Amazon Craton, Brazil: varying styles of Archean through Paleoproterozoic to Neoproterozoic base- and precious-metal mineralisation. Ore Geol. Rev. 33, 451–489.

Hirata, W.K., Rigon, J.C., Kadekaru, K., Cordeiro, A.A.A.C., Meireles, E.A., 1982. Geologia regional da Província Mineral de Carajás, in: SBG/NO. Presented at the Simpósio de Geologia da Amazônia 1, Belém, pp. 100–110.

Hitzman, M.W., Oreskes, N., Einaudi, M.T., 1992. Geological characteristics and tectonic setting of Proterozoic iron oxide (Cu-U-Au-REE) deposits. Precambrian Res. 58, 241–287.

Holdsworth, R.E., Pinheiro, R.V.L., 2000. The anatomy of shallowcrustal transpressional structures: Insights from the Archean Carajás fault zone, Amazon, Brazil. J. Struct. Geol. 22, 1105–1123.

Huhn, S.R.B., Nascimento, J.A.S., 1997. São os depósitos cupríferos de Carajás do tipo Cu-Au-U-ETR? SBG, Contribuições a geologia da Amazônia 1, 143–160.

Huhn, S.R.B., Souza, C.I.J., Albuquerque, M.C., Leal, E.D., Brustolin, V., 1999. Descoberta do depósito Cu-(Au) Cristalino: Geologia e mineralização associada região da Serra do Rabo-Carajás-PA.

Hunger, R.B., Xavier, R.P., Moreto, C.P.N., Gao, J.-F., 2018. Hydrothermal Alteration, Fluid Evolution, and Re-Os Geochronology of the Grota Funda Iron Oxide

Copper-Gold Deposit, Carajás Province (Pará State), Brazil. Econ. Geol. 113, 1769–1794. https://doi.org/10.5382/econgeo.2018.4612

Leake, B.E., Woolley, A.R., Arps, C.E.S., Birch, W.D., Gilbert, M.C., Grice, J.D., Hawthorne, F.C., Kato, A., Kisch, H.J., Krivovichev, V.G., Linthout, K., Laird, J., Mandarino, J.A., Maresch, W.V., Nickel, E.H., Rock, N.M.S., Schumacher, J.C., Smith, D.C., Stephenson, N.C.N., Ungaretti, L., Whittaker, E.J.W., Guo Youzhi, 1997. Nomenclature of amphiboles; report of the subcommittee on amphiboles of the International Mineralogical Association, Commission on New Minerals and Mineral Names. Can. Mineral. 35, 219–246.

Lindenmayer, Z.G., 2003. Depósito de Cu–Au do Salobo, Serra dos Carajás: Uma revisão, in: Caracterização e Modelamento de Depósitos Minerais, Ronchi L.H., Althoff F.J. Editora Unisinos, São Leopoldo, pp. 69–98.

Lindenmayer, Z.G., 1990. Salobo Sequence, Carajás, Brazil: Geology, Geochemistry And Metamorphism (Mestrado). University of Western Ontario, Ontario - Canada.

Lindenmayer, Z.G., Fyfe, W.S., 1994. The Salobo Cu (Au, Ag, Mo) Deposit, Serra dos Carajás, Brazil.

Lindenmayer, Z.G., Teixeira, J.B.G., 1999. Ore genesis at the Salobo copper deposit, Serra dos Carajás, in: Base Metal Deposits of Brazil. Silva MG, Misi A, MME/CPRM/DNPM, Brasília, pp. 33–43.

Locock, A.J., 2014. An Excel spreadsheet to classify chemical analyses of amphiboles following the IMA 2012 recommendations. Comput. Geosci. 62, 1–11. https://doi.org/10.1016/j.cageo.2013.09.011

Machado, N., Krough, T.E., Lindenmayer, Z.G., 1991. U–Pb geochronology of Archean magmatism and basement reactivation in the Carajás Area, Amazon Shield, Brazil. Precambrian Res. 49, 1–26.

Marschik, R., Mathur, R., Ruiz, J., Leveille, R.A., Almeida, A.-J. de, 2005. Late Archean Cu-Au-Mo mineralization at Gameleira and Serra Verde, Carajàs Mineral Province, Brazil: constraints from Re-Os molybdenite ages. Miner. Deposita 39, 983–991.

Marshall, B., Gilligan, L.B., 1993. Remobilization, syn-tectonic processes and massive sulphide deposits. Struct. Setting Controls Miner. Depos. 8, 39–64. https://doi.org/10.1016/0169-1368(93)90027-V

Marshall, B., Vokes, F.M., Larocque, A.C.L., 1998. Regional Metamorphic Remobilization: Upgrading and Formation of Ore Deposits. Rev. Econ. Geol., Metamorphic and metamorphogenic ore deposits 11, 19–38.

Melo, G.H.C. de, 2018. Temporal evolution and source of fluids of the Salobo and Igarapé Bahia IOCG deposits, Carajás Province (Ph.D.). Universidade Estadual de Campinas, Campinas.

Melo, G.H.C. de, 2014. Evolução Temporal do Depósito de Óxido de Ferro-Cobre-Ouro de Salobo, Província Carajás (Mestrado). Universidade Estadual de Campinas, Campinas.

Melo, G.H.C. de, Monteiro, L.V.S., Xavier, R.P., Moreto, C.P.N., Santiago, É.S.B., Dufrane, S.A., Aires, B., Santos, A.F.F., 2017. Temporal evolution of the giant Salobo IOCG deposit, Carajás Province (Brazil): constraints from paragenesis of hydrothermal alteration and U-Pb geochronology. Miner. Deposita 52, 733–746. https://doi.org/10.1007/s00126-016-0700-x

Moreto, C.P.N., 2013. Geocronologia U-Pb e Re-Os aplicada à evolução metalogenética do Cinturão Sul do Cobre da Província Mineral de Carajás (Ph.D.). Universidade Estadual de Campinas, Campinas.

Moreto, C.P.N., 2010. O depósito de óxido de ferro-cobre-ouro Bacaba, Província Mineral de Carajás: Geocronologia U-Pb das rochas hospedeiras (Mestrado). Universidade Estadual de Campinas, Campinas.

Moreto, C.P.N., Monteiro, L.V.S., Xavier, R.P., Amaral, W.S., Santos, T.J.S., Juliani, C., Souza Filho, C.R. de, 2011. Mesoarchean (3.0 and 2.86 Ga) host rocks of the iron oxide-Cu-Au Bacaba deposit, Carajás Mineral province: U-Pb geochronology and metallogenetic implications. Miner. Deposita 46, 789–811.

Moreto, C.P.N., Monteiro, L.V.S., Xavier, R.P., Creaser, R.A., Dufrane, S.A., Melo, G.H.C. de, da Silva, M.A.D., Tassinari, C.C.G., Kei, S., 2015a. Timing of multiple hydrothermal events in the iron oxide–copper–gold deposits of the Southern Copper Belt, Carajás Province, Brazil. Miner. Deposita.

Moreto, C.P.N., Monteiro, L.V.S., Xavier, R.P., Creaser, R.A., Dufrane, S.A., Tassinari, C.C.G., Sato, K., Kemp, A.I.S., Amaral, W.S., 2015b. Neoarchean and Paleoproterozoic Iron Oxide-Copper-Gold Events at the Sossego Deposit, Carajás Province, Brazil: Re-Os and U-Pb Geochronological Evidence. Econ. Geol. 110, 809–835.

Nogueira, A.C.R., Truckenbrodt, W., Pinheiro, R.V.L., 1995. Formação águas claras, Pré-cambriano da serra dos carajás: redescrição e redefinição litoestratigráfica. Bol Mus Para. Emílio Goeldi Ciências da Terra 7, 177–277.

Olszewski, W.J., Wirth, K.R., Gibbs, A.K., Gaudette, H.E., 1989. The age, origin, and tectonics of the Grão Pará group and associated rocks, Serra dos Carajás, Brazil: Archean continental vulcanism and rifting. Precambrian Res. 42, 229–254.

Pidgeon, R.T., Macambira, M.J.B., Lafon, J.M., 2000. Th-U-Pb isotopic systems and internal structures of complex zircons from an enderbite from the Pium Complex, Carajás province, Brazil: Evidence for the ages of granulite facies metamorphism and the protolith of the enderbite. Chem. Geol. 166, 159–171.

Pinheiro, R.V.L., 1997. Reactivation history of the Carajás and Cinzento Strike-Slip system, Amazon, Brazil (Ph.D.). University of Durham.

Pinheiro, R.V.L., Holdsworth, R.E., 1997. Reactivation of Archaean strike-slip fault systems, Amazon region, Brazil. J. Geol. Soc. 154, 99–103.

Pollard, P.J., Taylor, R.G., Peters, L., Matos, F., Freitas, C., Saboia, L., Huhn, S., 2018. 40Ar-39Ar dating of Archean iron oxide Cu-Au and Paleoproterozoic granite-related Cu-Au deposits in the Carajás Mineral Province, Brazil: implications for genetic models. Miner. Deposita 1–18.

Requia, K., 1995. O Papel do metamorfismo e fases fluidas na gênese da mineralização de cobre de Salobo, Província Mineral de Carajás, Pará. (Mestrado). Universidade Estadual de Campinas, Campinas.

Requia, K., Fontboté, L., 2000. The Salobo Iron Oxide Copper-Gold Deposit, Carajás, Northern Brazil. Hydrothermal Iron Oxide Copp.-Gold Relat. Depos. Glob. Perspect. 1, 225–236.

Requia, K., Fontboté, L., 1999. Hydrothermal alkali metasomatism in the Salobo iron oxide Cu (-Au) deposit, Carajás Mineral Province, northern Brazil. CJ Stanley Al Mineral deposits: processes to processing, 1025–1028.

Requia, K., Stein, H., Fontboté, L., Chiaradia, M., 2003. Re-Os and Pb-Pb geochronology of the Archean Salobo iron oxide copper-gold deposit, Carajás mineral province, northern Brazil. Miner. Deposita 38, 727–738. https://doi.org/10.1007/s00126-003-0364-1

Roseboom Jr, E.H., 1966. An investigation of the system Cu-S and some natural copper sulfides between 25° and 700°C. Econ. Geol. 61 nº4, 641–672.

Santos, J.O.S., 2003. Geotectônica do Escudo das Guianas e Brasil-Central, in: Geologia, Tectônica e Recursos Minerais Do Brasil: Texto, Mapas e SIG. CPRM, pp. 169–226.

Sardinha, A.S., Barros, C.E.M., Krymsky, M., 2006. Geology, geochemistry and U-Pb geochronology of the Archean (2.74 Ga) Serra do Rabo granite stocks, Carajás metallogenetic province, northern Brazil. J. South Am. Earth Sci. 20, 327–339.

Silva, A.R.C., Villas, R.N., Lafon, J.M., Craveiro, G.S., 2012. Idade da alteração e mineralização do depósito de Cu-Au Visconde, Província Mineral de Carajás (Pará), Brasil.

Silva, M.A.D., 2014. Metatexitos e diatexitos do Complexo Xingu na região de Canaã dos Carajás: implicações para a evolução mesoarqueana do Domínio Carajás (Mestrado). Universidade Estadual de Campinas, Campinas.

Silva, M.G., Teixeira, J.B.G., Pimentel, M.M., Vasconcelos, P.M., Arielo, A., Rocha, W.J.S.F., 2005. Geologia e mineralizações de Fe-Cu-Au do Alvo GT46 (Igarapé Cinzento), Carajás, in: Caracterização de Depósitos Minerais Em Distritos Mineiros Da Amazônia. DMNP-CT-mineral/FINEPADIMB, pp. 94–151.

Soares, A.D.V., Macambira, M.J.B., Santos, M.G.S., Vieira, E.A.P., Massoti, F.S., Souza, C.I.J., Padilha, J.L., Magni, M.C.V., 2001. Depósito Cu-(Au) Cristalino, Serra dos Carajás, PA: Idade da mineralização com base em análises Pb-Pb em sulfetos (dados preliminares).

Souza, S.R.B., Macambira, M.J.B., Sheller, T., 1996. Novos dados geocronológicos para os granitos deformados do Rio Itacaiúnas (Serra dos Carajás, PA); implicações estratigráficas.

Tassinari, C.C.G., Mellito, K.M., Babinski, M., 2003. Age and origin of the Cu (Au-Mo-Ag) Salobo 3A ore deposit, Carajás Mineral Province, Amazonian Craton, northern Brazil. Episodes 26, no.1.

VALE, 2018. Produção e vendas da Vale no 3T18 (Comunicado de Produção e Vendas).

VALE, 2012. Vale obtains operation license for Salobo [WWW Document]. URL http://saladeimprensa.vale.com/en/release/interna.asp?id=22000

Vasquez, L.V., Rosa-Costa, L.R., Silva, C.G., Ricci, P.F., Barbosa, J.O., Klein, E.L., Lopes, E.S., Macambira, E.B., Chaves, C.L., Carvalho, J.M., Oliveira, J.G., Anjos, G.C., Silva, H.R., 2008. Geologia e Recursos Minerais do Estado do Pará: Sistema de Informações Geográficas —SIG: texto explicativo dos mapas Geológico e Tectônico e de Recursos Minerais do Estado do Pará Organizadores, Vasquez ML, Rosa-Costa LT. 1:1.000.000. CPRM, Belém.

Xavier, R.P., Monteiro, L.V.S., Moreto, C.P.N., Pestilho, A.L.S., Melo, G.H.C. de, da Silva, M.A.D., Aires, B., Ribeiro, C., e Silva, F.H.F., 2012. The Iron Oxide Copper-Gold Systems of the Carajás Mineral Province, Brazil, in: Geology and Genesis of Major Copper Deposits and Districts of the World: A Tribute to Richard H. Sillitoe., Society Economic Geologists Special Publication. J.W. Hedenquist, M. Harris, and F. Camus, pp. 433–454.

Yund, R.A., Kullerud, G., 1966. Thermal Stability of Assemblages in the Cu-Fe-S System. J. Petrol. 7, 454–488.

4 Conclusão

O depósito de Salobo tem uma história complexa e que inclui eventos hidrotermais e metamórficos superpostos, além de estar associado a intrusões graníticas e uma grande zona de cisalhamento transcorrente. Todos esses fatos contribuem para uma bibliografa sobre o local que está em constante mudança e evolução acerca da classificação, fonte de metais, protólitos, rochas hospedeiras, gênese e alterações hidrotermais de Salobo. Contudo, estudos petrográficos em diferentes litotipos e de química mineral, quando associados ao conhecimento acumulado na área tornam possível a elaboração de nova proposta de sequência paragenética e de eventos que melhor explicam a evolução do depósito em relação a texturas e mineralogia observados. Essa evolução é caracterizada por um evento fonte principal de mineralização (2,73 Ga) em que aconteceu o estágio IOCG da gênese e um outro intenso evento posterior de remobilização metamórfica do minério fonte.

No contexto de formação de depósito fonte tipo IOCG, um enriquecimento em sódio inicial (Na-scapolita) evolui para alteração com enriquecimento de cálcio e ferro (hornblenda, Fe-actinolita, magnetita, apatita, ilvaíta). O enriquecimento em ferro também resulta em porções com alta cimentação de magnetita e uma assembleia mineral com ferrossilite, grunerita e faialita em parte da brecha. Posteriormente entrada rápida de grande quantidade de fluido sulfetado promove brechação e consequente cristalização de matriz de calcopirita, formando uma brecha hidrotermal. Esse fluido sulfetado é enriquecido em Cu, Fe, Co, Ni, Zn e Pb. Resfriamento do fluido sulfetado que inicialmente estava a alta temperatura promove separação de fases na solução sólida da calcopirita, resultando na cristalização de pirita e possivelmente bornita. Diferenciação de zonas ricas em níquel nos cristais de pirita são promovidas pela diminuição da capacidade de incorporação de níquel na estrutura da pirita por causa do resfriamento. Portanto a mineralização fonte principal é do tipo IOCG com minério formado predominantemente por calcopirita.

Reativação da Zona de Cisalhamento Cinzento em 2,5 Ga, afetou as rochas do depósito e resultou em um conjunto de falhas transcorrentes, criando um corredor de alta tensão e deformação onde granada-biotita xisto foi formado. Lentes de brecha com matriz de calcopirita formada no estágio IOCG anterior foram preservadas em planos de inflexão onde ficaram parcialmente protegidas das altas pressões causadas pela movimentação das falhas. Subsequente influxo de magnetita transformou grande parte do granada-biotita xisto em magnetita xisto.

Remobilização metamórfica do minério fonte foi promovida por fluidos hidrotermais de baixa temperatura e alto conteúdo F e CO_2. Esse fluido foi canalizado pelas falhas do depósito e interagiu com as rochas por meio dos sistemas de veio. Resfriamento dos sulfetos ricos em cobre que foram precipitados nos veios, os quais são parte da solução sólida da bornita, resultou em

texturas mimerquítica entre bornita e calcocita a partir da exsolução das fases. Esses processos são, possivelmente, ligados a colocação de granitos tipo-A na Província Carajás (1,8 – 1,9 Ga).

5 Referências Bibliográficas

Barros, C.E.M., Sardinha, A.S., Barbosa, J.P.O., Macambira, M.. J.B., 2009. Structure, petrology, geochemistry and zircon U/Pb and Pb/Pb geochronology of t e synkinematic Archean (2.7 Ga) A-type granites from the Carajás metallogenic province, northern Brazil. Can. Mineral. 47, 1423–1440.

Cabri, L.J., 1973. New Data on Phase Relations in the Cu-Fe-S S ystem. Econ. Geol. 68, 443–454.

Chakrabarti, D.J., Laugghlin, D.E., 1983. The Cu-S (Copper-Sulfur) System. Bull. Alloy Phase Diagr. 4 nº3, 254–271.

Ciobanu, C.L., Cook, N.J., Ehrig, K., 2017. Ore minerals down to the nanoscale: Cu-(Fe)-sulphides from the iron oxide copper gold deposit at Olympic Dam, South Australia. Ore Geol. Rev. 81, 1218–1235.

Cook, N.J., Ciobanu, C.L., Danyushevsky, L.V., Gilbert, S., 2011. Minor and trace elements in bornite and associated Cu–(Fe)-sulfides: A LA-ICP-MS studyBornite mineral chemistry. Geochim. Cosmochim. Acta 75, 6473–6496. https://doi.org/10.1016/j.gca.2011.08.021

Craig, J.R., Scott, D., 1974. Sulfide Phase Equilibria, in: Sulfide Mineralogy, Sulfide Mineralogy. Reviews in Mineralogy, p. Chapter 5, CS-1-CS-110.

Craig, J.R., Vaughan, D.J., 1990. Compositional and textural variations of the major iron and base-metal sulphide minerals, in: Sulphide Deposits-Their Origin and Processing. P.M.J. Gray, G.J. Bowyer, J.F Castle, D.J . Vaughan and N.A. Warner (eds). The Institution of Mining and Metallurgy, pp. 1–16.

de Freitas Toledo, P.I., Penteado Natividade Moreto, C., Xavier, R.P., Gao, J., da Silva Nogueira de Matos, J.H., de Melo, G.H.C., 2019. Multistage Evolution of the Neoarchean (ca. 2.7 Ga) Igarapé Cinzento (GT-46) Iron Oxide Copper-Gold Deposit, Cinzento Shear Zone, Carajás Province, Brazil. Econ. Geol. 114, 1–34. https://doi.org/10.5382/econgeo.2019.4617

DOCEGEO, 1988. Revisão litoestratigráfica da Província Mineral de Carajás - Litoestratigrafia e principais depósitos minerais.

Domingos, F.H.G., 2009. The structural setting of the Canaã dos Carajás region and Sossego-Sequeirinho deposits, Carajás, Brazil (Ph.D.). Durhan University, Durhan, United Kingdom.

Feio, G.R.L., Dall'Agnol, R., Dantas, E.L., Macambira, M.J.B., Gomes, A.C.B., Sardinha, A.S., Oliveira, D.C., Santos, R.D., Santos, P.A., 2012. Geochemistry, geochronology, and origin of the Neoarchean Planalto Granite suite, Carajás, Amazonian craton: A-type or hydrated charnockitic granites? Lithos 151, 57–73.

Feio, G.R.L., Dall'Agnol, R., Dantas, E.L., Macambira, M.J.B., Santos, J.O.S., Althoff, F.J., Soares, J.E.B., 2013. Archean granitoid magmatism in the Canaã dos Carajás area: implications for crustal evolution of the Carajás province, Amazonian craton, Brazil. Precambrian Res. 227, 157-.

Fernandez, O.J.C., 2002. Microquímica e mineralogia de processos do minério de cobre de Salobo, Carajás (Mestrado). Universidade Federal do Pará, Belém.

Ferreira Filho, C.F., Cançado, F., Correa, C., Macambira, E.M.B., Junqueira-Brod, T.C., Siepierski, L., 2007. Mineralizações estratiformes de PGENi associadas a complexos acamadados em Carajás: os exemplos de Luanga e Serra da Onça, in:

Contribuições à Geologia Da Amazônia. Rosa Costa L. T., Klein E.L., Viglio E.P., SBG-Núcleo Norte, Belém, pp. 1–14.

Gibbs, A.K., Wirth, K.R., Hirata, W.K., Olszewski, W.J., 1986. Age and composition of the Grão Pará Group volcanics, Serra dos Carajás. Rev. Bras. Geociências 16, 201–211.

Grainger, C.J., Tallarico, F.H.B., Fletcher, I.R., 2008. Metallogenesis of the Carajás Mineral Province, Southern Amazon Craton, Brazil: varying styles of Archean through Paleoproterozoic to Neoproterozoic base- and precious-metal mineralisation. Ore Geol. Rev. 33, 451–489.

Hirata, W.K., Rigon, J.C., Kadekaru, K., Cordeiro, A.A.A.C., Meireles, E.A., 1982. Geologia regional da Província Mineral de Carajás, in: SBG/NO. Presented at the Simpósio de Geologia da Amazônia 1, Belém, pp. 100–110.

Hitzman, M.W., Oreskes, N., Einaudi, M.T., 1992. Geological characteristics and tectonic setting of Proterozoic iron oxide (Cu-U-Au-REE) deposits. Precambrian Res. 58, 241–287.

Holdsworth, R.E., Pinheiro, R.V.L., 2000. The anatomy of shallowcrustal transpressional structures: Insights from the Archean Carajás fault zone, Amazon, Brazil. J. Struct. Geol. 22, 1105–1123.

Huhn, S.R.B., Nascimento, J.A.S., 1997. São os depósitos cupríferos de Carajás do tipo Cu-Au-U-ETR? SBG, Contribuições a geologia da Amazônia 1, 143–160.

Huhn, S.R.B., Souza, C.I.J., Albuquerque, M.C., Leal, E.D., Brustolin, V., 1999. Descoberta do depósito Cu-(Au) Cristalino: Geologia e mineralização associada região da Serra do Rabo-Carajás-PA.

Hunger, R.B., Xavier, R.P., Moreto, C.P.N., Gao, J.-F., 2018. Hydrothermal Alteration, Fluid Evolution, and Re-Os Geochronology of the Grota Funda Iron Oxide Copper-Gold Deposit, Carajás Province (Pará State), Brazil. Econ. Geol. 113, 1769–1794. https://doi.org/10.5382/econgeo.2018.4612

Leake, B.E., Woolley, A.R., Arps, C.E.S., Birch, W.D., Gilbert, M.C., Grice, J.D., Hawthorne, F.C., Kato, A., Kisch, H.J., Krivovichev, V.G., Linthout, K., Laird, J., Mandarino, J.A., Maresch, W.V., Nickel, E.H., Rock, N.M.S., Schumacher, J.C., Smith, D.C., Stephenson, N.C.N., Ungaretti, L., Whittaker, E.J.W., Guo Youzhi, 1997. Nomenclature of amphiboles; report of the subcommittee on amphiboles of the International Mineralogical Association, Commission on New Minerals and Mineral Names. Can. Mineral. 35, 219–246.

Lindenmayer, Z.G., 2003. Depósito de Cu–Au do Salobo, Serra dos Carajás: Uma revisão, in: Caracterização e Modelamento de Depósitos Minerais, Ronchi L.H., Althoff F.J. Editora Unisinos, São Leopoldo, pp. 69–98.

Lindenmayer, Z.G., 1990. Salobo Sequence, Carajás, Brazil: Geology, Geochemistry And Metamorphism (Mestrado). University of Western Ontario, Ontario - Canada.

Lindenmayer, Z.G., Fyfe, W.S., 1994. The Salobo Cu (Au, Ag, Mo) Deposit, Serra dos Carajás, Brazil.

Lindenmayer, Z.G., Teixeira, J.B.G., 1999. Ore genesis at the Salobo copper deposit, Serra dos Carajás, in: Base Metal Deposits of Brazil. Silva MG, Misi A, MME/CPRM/DNPM, Brasília, pp. 33–43.

Locock, A.J., 2014. An Excel spreadsheet to classify chemical analyses of amphiboles following the IMA 2012 recommendations. Comput. Geosci. 62, 1–11. https://doi.org/10.1016/j.cageo.2013.09.011

Machado, N., Krough, T.E., Lindenmayer, Z.G., 1991. U–Pb geochronology of Archean magmatism and basement reactivation in the Carajás Area, Amazon Shield, Brazil. Precambrian Res. 49, 1–26.

Marschik, R., Mathur, R., Ruiz, J., Leveille, R.A., Almeida, A.-J. de, 2005. Late Archean Cu-Au-Mo mineralization at Gameleira and Serra Verde, Carajàs Mineral Province, Brazil: constraints from Re-Os molybdenite ages. Miner. Deposita 39, 983–991.

Marshall, B., Gilligan, L.B., 1993. Remobilization, syn-tectonic processes and massive sulphide deposits. Struct. Setting Controls Miner. Depos. 8, 39–64. https://doi.org/10.1016/0169-1368(93)90027-V

Marshall, B., Vokes, F.M., Larocque, A.C.L., 1998. Regional Metamorphic Remobilization: Upgrading and Formation of Ore Deposits. Rev. Econ. Geol., Metamorphic and metamorphogenic ore deposits 11, 19–38.

Melo, G.H.C. de, 2018. Temporal evolution and source of fluids of the Salobo and Igarapé Bahia IOCG deposits, Carajás Province (Ph.D.). Universidade Estadual de Campinas, Campinas.

Melo, G.H.C. de, 2014. Evolução Temporal do Depósito de Óxido de Ferro-Cobre-Ouro de Salobo, Província Carajás (Mestrado). Universidade Estadual de Campinas, Campinas.

Melo, G.H.C. de, Monteiro, L.V.S., Xavier, R.P., Moreto, C.P.N., Santiago, É.S.B., Dufrane, S.A., Aires, B., Santos, A.F.F., 2017. Temporal evolution of the giant Salobo IOCG deposit, Carajás Province (Brazil): constraints from paragenesis of hydrothermal alteration and U-Pb geochronology. Miner. Deposita 52, 733–746. https://doi.org/10.1007/s00126-016-0700-x

Moreto, C.P.N., 2013. Geocronologia U-Pb e Re-Os aplicada à evolução metalogenética do Cinturão Sul do Cobre da Província Mineral de Carajás (Ph.D.). Universidade Estadual de Campinas, Campinas.

Moreto, C.P.N., 2010. O depósito de óxido de ferro-cobre-ouro Bacaba, Província Mineral de Carajás: Geocronologia U-Pb das rochas hospedeiras (Mestrado). Universidade Estadual de Campinas, Campinas.

Moreto, C.P.N., Monteiro, L.V.S., Xavier, R.P., Amaral, W.S., Santos, T.J.S., Juliani, C., Souza Filho, C.R. de, 2011. Mesoarchean (3.0 and 2.86 Ga) host rocks of the iron oxide-Cu-Au Bacaba deposit, Carajás Mineral province: U-Pb geochronology and metallogenetic implications. Miner. Deposita 46, 789–811.

Moreto, C.P.N., Monteiro, L.V.S., Xavier, R.P., Creaser, R.A., Dufrane, S.A., Melo, G.H.C. de, da Silva, M.A.D., Tassinari, C.C.G., Kei, S., 2015a. Timing of multiple hydrothermal events in the iron oxide–copper–gold deposits of the Southern Copper Belt, Carajás Province, Brazil. Miner. Deposita.

Moreto, C.P.N., Monteiro, L.V.S., Xavier, R.P., Creaser, R.A., Dufrane, S.A., Tassinari, C.C.G., Sato, K., Kemp, A.I.S., Amaral, W.S., 2015b. Neoarchean and Paleoproterozoic Iron Oxide-Copper-Gold Events at the Sossego Deposit, Carajás Province, Brazil: Re-Os and U-Pb Geochronological Evidence. Econ. Geol. 110, 809–835.

Nogueira, A.C.R., Truckenbrodt, W., Pinheiro, R.V.L., 1995. Formação águas claras, Pré-cambriano da serra dos carajás: redescrição e redefinição litoestratigráfica. Bol Mus Para. Emílio Goeldi Ciências da Terra 7, 177–277.

Olszewski, W.J., Wirth, K.R., Gibbs, A.K., Gaudette, H.E., 1989. The age, origin, and tectonics of the Grão Pará group and associated rocks, Serra dos Carajás, Brazil: Archean continental vulcanism and rifting. Precambrian Res. 42, 229–254.

Pidgeon, R.T., Macambira, M.J.B., Lafon, J.M., 2000. Th-U-Pb isotopic systems and internal structures of complex zircons from an enderbite from the Pium Complex, Carajás province, Brazil: Evidence for the ages of granulite facies metamorphism and the protolith of the enderbite. Chem. Geol. 166, 159–171.

Pinheiro, R.V.L., 1997. Reactivation history of the Carajás and Cinzento Strike-Slip system, Amazon, Brazil (Ph.D.). University of Durham.

Pinheiro, R.V.L., Holdsworth, R.E., 1997. Reactivation of Archaean strike-slip fault systems, Amazon region, Brazil. J. Geol. Soc. 154, 99–103.

Pollard, P.J., Taylor, R.G., Peters, L., Matos, F., Freitas, C., Saboia, L., Huhn, S., 2018. 40Ar-39Ar dating of Archean iron oxide Cu-Au and Paleoproterozoic granite-related Cu-Au deposits in the Carajás Mineral Province, Brazil: implications for genetic models. Miner. Deposita 1–18.

Requia, K., 1995. O Papel do metamorfismo e fases fluidas na gênese da mineralização de cobre de Salobo, Província Mineral de Carajás, Pará. (Mestrado). Universidade Estadual de Campinas, Campinas.

Requia, K., Fontboté, L., 2000. The Salobo Iron Oxide Copper-Gold Deposit, Carajás, Northern Brazil. Hydrothermal Iron Oxide Copp.-Gold Relat. Depos. Glob. Perspect. 1, 225–236.

Requia, K., Fontboté, L., 1999. Hydrothermal alkali metasomatism in the Salobo iron oxide Cu (-Au) deposit, Carajás Mineral Province, northern Brazil. CJ Stanley Al Mineral deposits: processes to processing, 1025–1028.

Requia, K., Stein, H., Fontboté, L., Chiaradia, M., 2003. Re-Os and Pb-Pb geochronology of the Archean Salobo iron oxide copper-gold deposit, Carajás mineral province, northern Brazil. Miner. Deposita 38, 727–738. https://doi.org/10.1007/s00126-003-0364-1

Roseboom Jr, E.H., 1966. An investigation of the system Cu-S and some natural copper sulfides between 25° and 700°C. Econ. Geol. 61 nº4, 641–672.

Santos, J.O.S., 2003. Geotectônica do Escudo das Guianas e Brasil-Central, in: Geologia, Tectônica e Recursos Minerais Do Brasil: Texto, Mapas e SIG. CPRM, pp. 169–226.

Sardinha, A.S., Barros, C.E.M., Krymsky, M., 2006. Geology, geochemistry and U-Pb geochronology of the Archean (2.74 Ga) Serra do Rabo granite stocks, Carajás metallogenetic province, northern Brazil. J. South Am. Earth Sci. 20, 327–339.

Silva, A.R.C., Villas, R.N., Lafon, J.M., Craveiro, G.S., 2012. Idade da alteração e mineralização do depósito de Cu-Au Visconde, Província Mineral de Carajás (Pará), Brasil.

Silva, M.A.D., 2014. Metatexitos e diatexitos do Complexo Xingu na região de Canaã dos Carajás: implicações para a evolução mesoarqueana do Domínio Carajás (Mestrado). Universidade Estadual de Campinas, Campinas.

Silva, M.G., Teixeira, J.B.G., Pimentel, M.M., Vasconcelos, P.M., Arielo, A., Rocha, W.J.S.F., 2005. Geologia e mineralizações de Fe-Cu-Au do Alvo GT46 (Igarapé Cinzento), Carajás, in: Caracterização de Depósitos Minerais Em Distritos Mineiros Da Amazônia. DMNP-CT-mineral/FINEPADIMB, pp. 94–151.

Soares, A.D.V., Macambira, M.J.B., Santos, M.G.S., Vieira, E.A.P., Massoti, F.S., Souza, C.I.J., Padilha, J.L., Magni, M.C.V., 2001. Depósito Cu-(Au) Cristalino, Serra dos Carajás, PA: Idade da mineralização com base em análises Pb-Pb em sulfetos (dados preliminares).

Souza, S.R.B., Macambira, M.J.B., Sheller, T., 1996. Novos dados geocronológicos para os granitos deformados do Rio Itacaiúnas (Serra dos Carajás, PA); implicações estratigráficas.

Tassinari, C.C.G., Mellito, K.M., Babinski, M., 2003. Age and origin of the Cu (Au-Mo-Ag) Salobo 3A ore deposit, Carajás Mineral Province, Amazonian Craton, northern Brazil. Episodes 26, no.1.

VALE, 2018. Produção e vendas da Vale no 3T18 (Comunicado de Produção e Vendas).

VALE, 2012. Vale obtains operation license for Salobo [WWW Document]. URL http://saladeimprensa.vale.com/en/release/interna.asp?id=22000

Vasquez, L.V., Rosa-Costa, L.R., Silva, C.G., Ricci, P.F., Barbosa, J.O., Klein, E.L., Lopes, E.S., Macambira, E.B., Chaves, C.L., Carvalho, J.M., Oliveira, J.G., Anjos, G.C., Silva, H.R., 2008. Geologia e Recursos Minerais do Estado do Pará: Sistema de Informações Geográficas —SIG: texto explicativo dos mapas Geológico e Tectônico e de Recursos Minerais do Estado do Pará Organizadores, Vasquez ML, Rosa-Costa LT. 1:1.000.000. CPRM, Belém.

Xavier, R.P., Monteiro, L.V.S., Moreto, C.P.N., Pestilho, A.L.S., Melo, G.H.C. de, da Silva, M.A.D., Aires, B., Ribeiro, C., e Silva, F.H.F., 2012. The Iron Oxide Copper-Gold Systems of the Carajás Mineral Province, Brazil, in: Geology and Genesis of Major Copper Deposits and Districts of the World: A Tribute to Richard H. Sillitoe., Society Economic Geologists Special Publication. J.W. Hedenquist, M. Harris, and F. Camus, pp. 433–454.

Yund, R.A., Kullerud, G., 1966. Thermal Stability of Assemblages in the Cu-Fe-S System. J. Petrol. 7, 454–488.